


ORIGINAL ARTICLE

Addiction Biology

SSA

WILEY

Integration of pharmacochemistry, pharmacodynamics and metabolomics to reveal active ingredients and mechanism of Nan Bao detox capsule alleviating methamphetamine addiction

Bin Zhang^{1,2}  | Chen Yang^{1,2} | Yuxiao Zheng^{1,2} | Xinliang Li¹ | Xingguo Wang³ | Li Yuehui¹

¹Hunan Academy of Chinese Medicine, Changsha, China

²Hunan University of Chinese Medicine, Changsha, China

³Hunan Province Shaoyang Institution of TCM Detoxification, Shaoyang, China

Correspondence

Yuehui Li, Institute of Hunan Academy of Chinese Medicine, Changsha, 410000, China.
Email: 410256518@qq.com

Funding information

This work is supported by Hunan Provincial Natural Science Foundation-Pharmaceutical Joint Project (grant number 2020JJ9015) and Changsha Municipal Natural Science Foundation project (grant number KQ2402149).

Abstract

Nan Bao detox capsule (NBDC), derived from ancient Chinese opioid detox protocols, shows promising therapeutic potential in substance abuse disorders, particularly for attenuating methamphetamine (MA) addiction. This study aimed to identify active ingredients, evaluate therapeutic efficacy in an MA addiction rat model and delineate pharmacodynamic mechanisms using metabolomics. In vitro phytochemical profiling characterized 258 drug-related compounds, with 87 prototype entities mainly identified in rat plasma. NBDC significantly attenuated METH-induced behavioural anomalies and modulated neurotransmitter levels, notably increasing brain DA and serotonin (5-HT) content with concomitant upregulation of D1 dopamine receptor (DRD1) and 5-HT1A receptor (5-HT1AR) expression, ameliorating hippocampal pathology. Metabolomic analysis identified histamine receptor as a potential target and revealed the involvement of NBDC in metabolic pathways associated with cocaine addiction, amphetamine abuse and Parkinson's disease. Conclusively, NBDC presents a promising therapeutic agent for mitigating MA addiction through a synergistic interplay of multiple constituents, pharmacological targets and metabolic pathways.

KEYWORDS

Chinese herbal medicine, conditioned place preference, drug abuse, metabolomics, methamphetamine, pharmacodynamics

1 | INTRODUCTION

Methamphetamine (MA) serves as a potent synthetic stimulant of both the peripheral and central nervous systems, facilitating the release of dopamine, serotonin and norepinephrine from intracellular

Bin Zhang is the first author. Chen Yang is the co-author.

Bin Zhang and Chen Yang contributed equally to this work.

This is an open access article under the terms of the [Creative Commons Attribution-NonCommercial-NoDerivs](https://creativecommons.org/licenses/by-nc-nd/4.0/) License, which permits use and distribution in any medium, provided the original work is properly cited, the use is non-commercial and no modifications or adaptations are made.

© 2024 The Author(s). *Addiction Biology* published by John Wiley & Sons Ltd on behalf of Society for the Study of Addiction.

stores into the synaptic cleft, thereby inducing feelings of excitement and euphoria.¹ Chronic exposure to MA elevates the risk of neurological diseases such as Parkinson's disease, Alzheimer's disease and major depressive disorder. MA represents a highly addictive psychoactive substance with considerable potential for misuse. As reported in the 2023 China Drug Situation Report, METH is the most prevalent illicit drug in China, accounting for 50.8% of drug abuse incidents among 896 000 users. The 2024 World Drug Report indicates amphetamines rank as the third most commonly abused substance globally. The widespread misuse of METH poses a substantial challenge to the international healthcare sector. Despite treatment with antipsychotics such as risperidone, opioid substitution therapies like methadone and antibiotic interventions with ceftriaxone, a significant proportion of METH users experience relapse post-treatment. To date, the United States Food and Drug Administration has not approved any definitive therapeutic regimen for the management of METH withdrawal syndrome. Consequently, innovative strategies to combat METH addiction are in high demand.

Traditional Chinese Medicine (TCM) has been effectively utilized in China for over a century to cure opioid-induced withdrawal syndrome due to its high safety and non-addictive.² The monograph 'Jiu Mi Liang Fang' in TCM focuses on drug addiction rehabilitation, compiling treatment methods for opium poisoning, including avoidance of acid pills, opium prescriptions and smoking cessation prescriptions. Chinese herbal extracts such as levo-tetrahydropalmatine (l-THP) derived from *Corydalis*, pseudoginsenoside-F11 and ginsenoside Re from ginseng, as well as rhynchophylline from *Uncaria tomentosa*, have been documented for their protective effects against MA dependence.^{3–6} Clinically and experimentally, polyherbal formulations like Guiyuan Tablets, Fukang Tablets, Jitai Tablets, Jinniu Capsules and Shuhelian Xieyu capsules have been developed as new drugs as therapeutic options for MA dependence.⁷ However, the pharmacodynamic substance basis and mechanisms of action for these herbal remedies in treating MA addiction remain uncharacterized.

Leveraging its robust separation capabilities, rapid analysis speeds and exceptional sensitivity, ultra-performance liquid chromatography (UPLC) in tandem with high-resolution mass spectrometry (MS) serves as a powerful tool for the prediction and elucidation of unknown compound structures. For instance, Liu et al utilized UHPLC-Q-Orbitrap HRMS to annotate 138 constituents within walnut leaves, pinpointing 38 as potentially bioactive compounds.⁸ Similarly, Guan et al employed UHPLC-Q-Orbitrap HRMS to characterize 114 chemical components in *Polygonum capitatum*, identifying 68 organically absorbed exogenous substances—including 16 prototype compounds and 52 metabolites—within the plasma of hyperuricemic rats.⁹ This technique is especially adept at profiling bioactive constituents and compounds in biological matrices like blood and is particularly suitable for pharmaceutical and biomedical research.

Metabolomics occupies a leading position in biomedical innovation, offering the potential to uncover novel biomarkers and elucidate

both physiological and pathological processes.¹⁰ Sheng et al harnessed gas chromatography–mass spectrometry to identify four metabolites in serum as potential biomarkers from MA exposure.¹¹ An untargeted metabolomics approach combining serum and liver analyses revealed 10 potential metabolic biomarkers in mice with ethanol-induced gastric ulcers that had been administered polysaccharides from *Evodiae fructus*. These biomarkers are enriched to five significant metabolic pathways.¹² Such research advancements illustrate how metabolomics is not only instrumental in biomarker discovery but also increasingly pivotal in deciphering underlying biological mechanisms.

Nan Bao detox capsule (NBDC) has historically been utilized in the treatment of opioid dependency for many years. Prior animal studies conducted by our team demonstrated that NBDC effectively mitigates dependencies on morphine and MA, exhibiting safety profiles verified through acute and long-term toxicity assessments. Preliminary clinical investigations by our group indicated reduced scores for symptoms of withdrawal, anxiety and TCM syndromes in the treatment group, highlighting the therapeutic potential of NBDC for MA abstinence syndrome, particularly in cases with Qi and Yin deficiencies, toxin accumulation and stasis.¹³ Consequently, NBDC has been expanded to include a new indication for alleviating MA addiction. It has obtained authorization for preparation usage in medical facilities in Hunan, China, under the registration number (xiang-z20090939), and is currently being manufactured at scale, ensuring consistent quality. Quality control (QC) of the formulation is maintained through the use of a chromatographic fingerprint, as depicted in Figures S1 and S2 and Table 1. Clinically, NBDC has been implemented across 13 local drug rehabilitation centres, including those in Changsha, Shaoyang and Hengyang. Despite its therapeutic applications, the active constituents and the pharmacodynamic mechanism of NBDC remain unclear. Utilizing an animal model of MA addiction, this study endeavours to identify NBDC components that enter the bloodstream via UPLC-MS, investigate the pharmacodynamic influence of NBDC on the dopaminergic and serotonergic systems and explore the mechanism of action underlying the therapeutic effects of NBDC against MA addiction through metabolomics. This research will provide a scientifically grounded framework for guiding clinical applications of NBDC.

2 | MATERIALS AND METHODS

2.1 | Materials and reagents

MA was obtained from Shaoyang Addiction Treatment Centre (Shaoyang, China). NBDCs were supplied by Hunan Dekang Pharmaceutical Co. (Changsha, China, batch number: 200801). Risperidone, a positive drug, was purchased from Xi'an Janssen Pharmaceutical Co., Ltd. (Xi'an China, batch number: 190302047, specification: 1 mg per tablet).

Anti-dopamine receptor D1 and anti-5HT1A receptor antibodies were purchased from Abcam Plc (Cambridge, U.K.). The kits of DA

TABLE 1 The composition of the Nan Bao detox capsule.

No.	Chinese name	Medicinal part	Plant/animal/mineral name	Amount (g)
1	Huangqi	Root	<i>Astragalus membranaceus</i> (Fisch.) Bunge	90
2	Yuanzhi	Root	<i>Polygala tenuifolia</i> Willd.	90
3	Dangshen	Root	<i>Codonopsis pilosula</i> (Franch.) Nannf.	90
4	Renshen	Root and rhizome	<i>Panax ginseng</i> C. A. Mey.	90
5	Boziren	Seed	<i>Platycladus orientalis</i> (L.) Franco	90
6	Fushen	Sclerotium with pine root	<i>Poria cocos</i> (Schw.) Wolf	90
7	Suanzaoren	Seed	<i>Ziziphus jujuba</i> Mill.	90
8	Gouteng	Hooked stems	<i>Uncaria rhynchophylla</i> (Miq.) Miq. ex Havil.	90
9	Yanhusuo	Tuber	<i>Corydalis yanhusuo</i> W. T. Wang	90
10	Danshen	Root and rhizome	<i>Salvia miltiorrhiza</i> Bunge	90
11	Ruxiang	Resin—artillery products	<i>Boswellia carteri</i> Birdw.	90
12	Moyao	Resin—artillery products	<i>Commiphora myrrha</i> (Nees) Engl.	90
13	Zhichuanwu	Tuber—artillery products	<i>Aconitum carmichaelii</i> Debeaux	60
14	Zhicaowu	Tuber—artillery products	<i>Aconitum kusnezoffii</i> Rchb.	60
15	Naoyanghua	Flower	<i>Rhododendron molle</i> G. Don	1.8
16	Quanxie	All animal body	<i>Buthus martensii</i> Karsch	60
17	Wugong	All animal body	<i>Scolopendra subspinipes mutilans</i> L. Koch	30
18	Zhusha	–	Cinnabaris, HgS	60
19	Hupo	–	Succinum	90
20	Fangfeng	Root	<i>Saposhnikovia divaricate</i> (Turcz.) Schischk.	90
21	Huangqin	Root	<i>Scutellaria baicalensis</i> Georgi	90
22	Gancao	Root and rhizome	<i>Glycyrrhiza uralensis</i> Fisch.	60

ELISA, 5-HT ELISA, BCA protein assay and SDS-PAGE gel and goat anti-rabbit IgG (H + L) (peroxidase/HRP conjugated) were purchased from Elabscience Biotechnology Co. (Wuhan, China). The kits of QuickBlock™ western solution, haematoxylin–eosin (HE) staining and DAB Horseradish Peroxidase Color Development were purchased from Beyotime Biotech Inc (Shanghai, China). Universal two-step detection kit was purchased from ZSGB Biotechnology Co. (Beijing, China). GAPDH Polyclonal antibody was purchased from Proteintech Group, Inc. (Wuhan, China).

NBDC is a typical Chinese medicine formulation of herbs, animals and minerals detailed in Table 1. The plant name has been checked with <http://www.theplantlist.org>. Each herb was tested in accordance with the Chinese Pharmacopoeia (2020 edition) and conformed to the regulations.

2.2 | Animal experiments

Sprague–Dawley rats (6 weeks of age, weighing 180–200 g, with specific pathogen-free [SPF] status, and an equal sex ratio of males and females) were obtained from Tianqin Biotechnology Co. Ltd. (Changsha, China), Licence No. SCXK [Xiang] 2019–0014. These animals were housed in an SPF-grade facility at the Chinese Medicine

Research Institute of Hunan Academy of Chinese Medicine, Laboratory Licence No. SYXK [Xiang] 2020–0008. The experimental protocol involving these animals was ethically reviewed and approved in accordance with internationally recognized guidelines for the care and use of laboratory animals, with the Ethics Approval Number 2021–0098.

According to body weight, 60 rats were randomly divided into six groups: blank group, model group, low-dose group, medium-dose group, high-dose group and positive group, each group consisted of 10 animals. Blood samples from the rats were collected and separated serum and plasma. The samples were preserved at -80°C . The serum was used for biochemical analysis, and the plasma was detected by UPLC-MS. The hippocampus tissues of the rats were harvested and stored at -80°C for western blot and fixed in 4% paraformaldehyde for pathological examination.

In analysing components absorbed into the blood study, the rats ($n = 6$) were intragastrically administrated by NBDC (6.48 g/kg) for 14 days. They were called the drug-containing group (medicated plasma group). Blood samples from the rats were collected, and the plasma was separated to detect by UPLC-MS.

In the metabolomics study, six plasma samples of the blank group, model group and high dose group (drug group) were randomly selected for metabolomics study by UPLC-MS.

2.3 | The analysis of NBDC components in blood and metabolomics study

2.3.1 | Sample preparation

In this study, 1-g NBDC samples and 100- μ L plasma samples were thoroughly blended with 400 μ L of cold methanol and acetonitrile (v/v, 1:1) by the vortex. Then, the mixtures were handled with sonication for 1 h in 4°C water, reacted at –20°C for 1 h and centrifuged at 16,000g at 4°C for 20 min. The supernatants were gathered and dried under a vacuum. The samples were redissolved by adding 200- μ L acetonitrile-aqueous solution (1:1, v/v) and centrifuged for 20 min at 4°C with a speed of 16,000g. The supernatant was used for UPLC-MS analysis.

2.3.2 | Conditions of UPLC-MS

The untargeted metabolomics and component analysis of the samples was performed on the UPLC-ESI-Triple-TOF 5600-MS system (UHPLC, Shimadzu Nexera X2 LC-30 AD, Shimadzu, Japan) coupled with Q-Exactive Plus (Thermo Scientific, San Jose, USA).

The samples were placed in a 4°C autosampler throughout the analysis and were separated using ACQUITY UPLC HSS T3 column (2.1 mm \times 100 mm \times 1.7 μ m, Waters). The flow rate was 0.3 mL/min, the injection volume was 5 μ L and the column temperature was 40°C. The mobile phase contained: A: 0.1% formic acid solution in water and B: 100% acetonitrile (ACN). The mobile phase gradient elution is shown in Table 2.

Both electrospray ionization (ESI) positive mode and negative mode were applied for MS data acquisition¹⁴. The ESI source conditions were set as follows: spray voltage: 3.8 kv (+), 3.2 kv (–); capillary temperature: 320 (\pm); sheath gas: 30 (\pm); aux gas: 5 (\pm); probe heater temperature: 350 (\pm); S-Lens RF level: 50. In MS only acquisition, the instrument was set to acquire over the m/z range 80–1200 Da. The full MS scans were acquired at a resolution of 70 000 at m/z 200 and 17 500 at m/z 200 for MS/MS scans. The maximum injection time was set to 100 ms for MS and 50 ms for MS/MS. The isolation window for MS2 was set to 2 m/z, and the normalized collision energy (stepped) was set as 27, 29 and 32 for fragmentation.

QC samples were prepared by mixing different and equal amounts of blank extracted plasma samples to represent the samples under analysis.

TABLE 2 The ratio of mobile phase.

Time (min)	The ratio of A (%)	The ratio of B (%)
0	0	100
0.1	0	100
12	25	75
13.5	60	40
15	60	40
15.1	0	100
18	0	100

2.3.3 | Data preprocessing and filtering

The raw MS data was pre-handled by MS-DIAL for peak alignment, peak area extraction and retention time (RT) correction. The metabolites were screened by accuracy mass (mass tolerance < 0.01 Da) and MS/MS data (mass tolerance < 0.02 Da) and compared with HMDB, PubChem, TCMSP, other public databases and the self-built metabolite standard library. In the extracted ion features, only the variables having more than 50% of the non-zero measurement values in at least one group were kept.

2.3.4 | Multivariate statistical analysis

R (version 4.0.3) and R packages were used for all multivariate data analysis and model building. The principal component analysis (PCA), partial least-square discriminant analysis (PLS-DA) and orthogonal partial least-square discriminant analysis (OPLS-DA) were used to establish the model and analyse the data. The value of variable importance prediction (VIP) in the model of OPLS-DA and the *p*-value from the two-tailed Student's test for two groups analysis or one-way analysis of variance (ANOVA) for multiple groups analysis were used to determine the discriminating metabolites. The score of VIP indicated the contribution of an element to the discrimination between two groups of samples. The *p*-value suggested whether the difference between groups is significant.

2.3.5 | Components absorbed into blood screening

The NBDC drug components were identified reference online databases such as PubChem, TCMSP and literatures of single medicinal ingredient analysis. The blood-absorbed prototype components were screened by VIP value and *p*-value and compared with the NBDC drug compositions to confirm the source of Chinese herbs.

2.3.6 | Differential metabolites screening

VIP value and *p*-value were used to screen the discriminating metabolites. Components with VIP values greater than 1.0 and *p*-values of less than 0.05 were considered statistically significant metabolites. The identified differential metabolites were subjected to cluster analysis.

2.3.7 | KEGG enrichment analysis

In order to recognize the involved biological signal pathways, the differential metabolite data were executed KEGG pathway analysis using the KEGG database (<http://www.kegg.jp>). Enriched KEGG pathways were regarded as statistically significant by a *p*-value of less than 0.05.

2.4 | The relieve effect of NBDC on MA addiction

2.4.1 | Rat modelling and drug administration

In our previous pilot experiments, we established three dosage groups of 5, 10 and 20 mg/kg to explore the optimal dosing regimen and cycle for inducing addiction to MA. The results indicated that after MA administration at 20 mg/kg for 14 days, the most significant damage was observed in the hippocampal region. Therefore, for the modelling method, except for the blank group, all other groups received intraperitoneal injections of 20 mg/kg MA for continuous modelling over 14 days. The low, medium and high doses of NBDC were set at 1.62, 3.24 and 6.38 g/kg, respectively, equivalent to half, one and two times the equivalent rat dose calculated based on the maximum clinical dose for humans. The drugs were dissolved to the required concentrations in purified water before administration via gavage. For the positive (risperidone) group, the dosage was set at 1.08 mg/kg, equivalent to twice the equivalent rat dose, and administered via gavage for 14 consecutive days.

2.4.2 | Ethology evaluation

Conditioned place preference¹⁵

The conditioned place preference (CPP) experimental box was home-made, and the experiment was divided into pre-conditioning phase, conditioning phase, testing phase and extinction phase. The pre-conditioning phase was from the first day to the third day. The middle partition of the CPP box was opened. The rats were put into the box to run freely and acclimatized once daily for 20 min each for 3 days. The residence time of the rats in the white box and the black box was recorded. It implied the natural preference tendency of the rats and helped select the non-naturally preferred side box as the companion drug box. The conditioning phase was from the fourth day to the 17th day. The model and treatment groups were injected intraperitoneally with MA, and the blank group was injected with

equal saline. The animals were put into the companion box with closed access; then, the experimental rats were conditioned to train for 30 min each time; after 8 h, equal amounts of saline were injected; then, the rats were put into the non-companion box to train for 30 min, and the training continued for 14 days. The elimination stage was from the 18th to the 31st day. Only saline or Nan Bao detoxification clear capsule was given, and the rats were not trained. The test phase was on the 32nd day. The animals were put into the CPP training box and observed the conditioned positional preference response. CPP score is based on activity time in the companion drug box. The specific modelling and administration methods are shown in Figure 1.

Stereotyped behaviour¹⁶

A stereotyped behaviour test was conducted using the following scale: if rats were stationary, little or normal movement, scoring zero; if rats were active, occasional to frequent movement, scoring one; if rats were active with episodes of repetitive forward head searching, scoring two; if rats were continuous forward head searching, scoring three; if rats were frequent repetitive rearing, side-to-side weaving or turning, scoring four; and if rats were episodes of rapid jerking side-to-side, circular or dorsoventral head movements, scoring five. Stereotyped behaviours were scored by a valuator unaware of the specific experimental conditions. After each MA injection, rats were placed at the centre of the empty cage for a 10-min adaptive period. Then, the stereotyped behaviours of each rat were scored every 10 min over the next 60 min by an observer blind to the treatments. The final score was from the average score.

Spontaneous locomotor activity

After 20 min of administration, the rats were placed in the YLS-1B multifunctional rat spontaneous activity recorder (Shandong Academy of Medical Sciences Equipment Station Products). And then, the instrument began to record the number of autonomous activities in rats within 10 min.

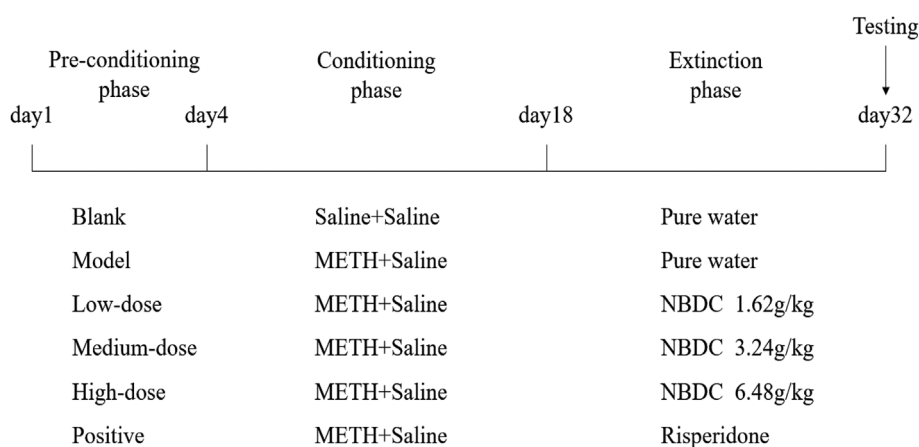


FIGURE 1 Conditioned place preference procedure.

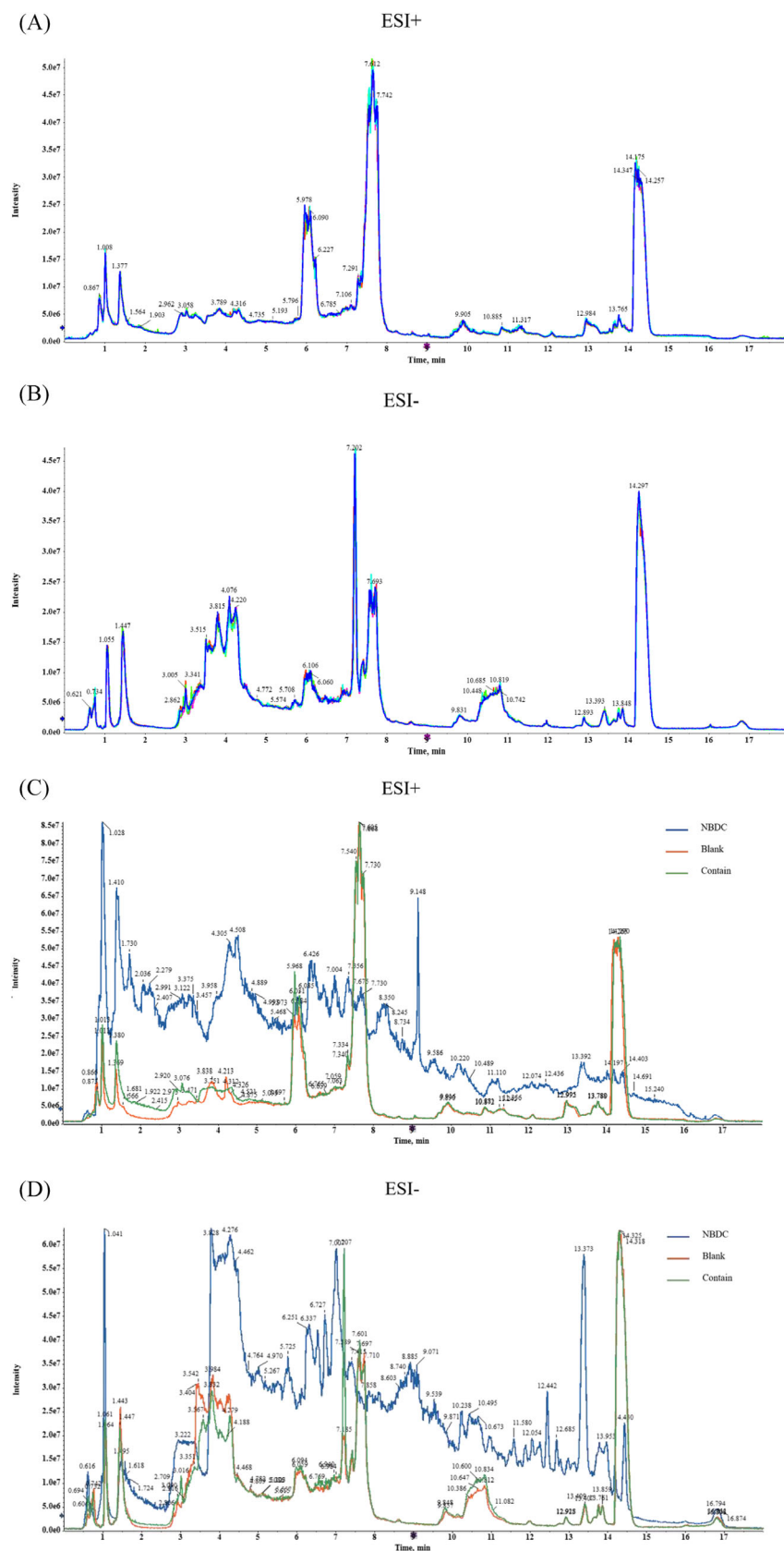


FIGURE 2 Total ion chromatograms in the positive and negative modes. (A) Positive model of QC samples. (B) Negative model of QC samples. (C) Positive model of NBDC and plasma samples. (D) Negative model of NBDC and plasma samples.

2.4.3 | Neurotransmitter and receptor changes

DA and 5-HT concentration changes

Blood was collected from rats, and the supernatant was centrifuged. The determination of DA or 5-HT concentration referred to the ELISA kit. The optical density (OD) value was measured at 450 nm using an enzyme calibrator.

DRD1 and 5-HT1A receptor expression changes

The expressions of DAD1 and HIT1A receptors in the hippocampus were detected by immunohistochemical staining (IHC) and western blot (WB) experiments. Immunoreactivity was quantified using the software of Image J to measure the mean OD positive cells. Densitometric analysis was performed using gel image scanner equipment (ChemiDoc XRS, Biorad, USA).

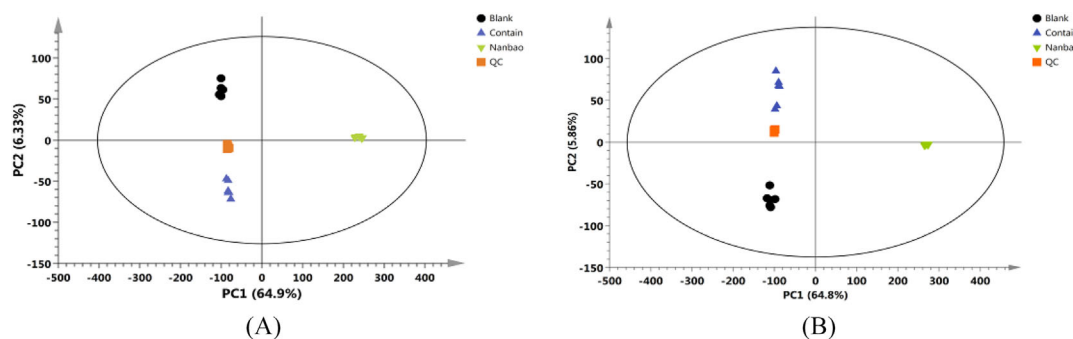


FIGURE 3 The score plots derived from principal component analysis in vivo and in vitro. (A) PCA score plot in the positive ion mode. (B) PCA score plot in the negative ion mode.

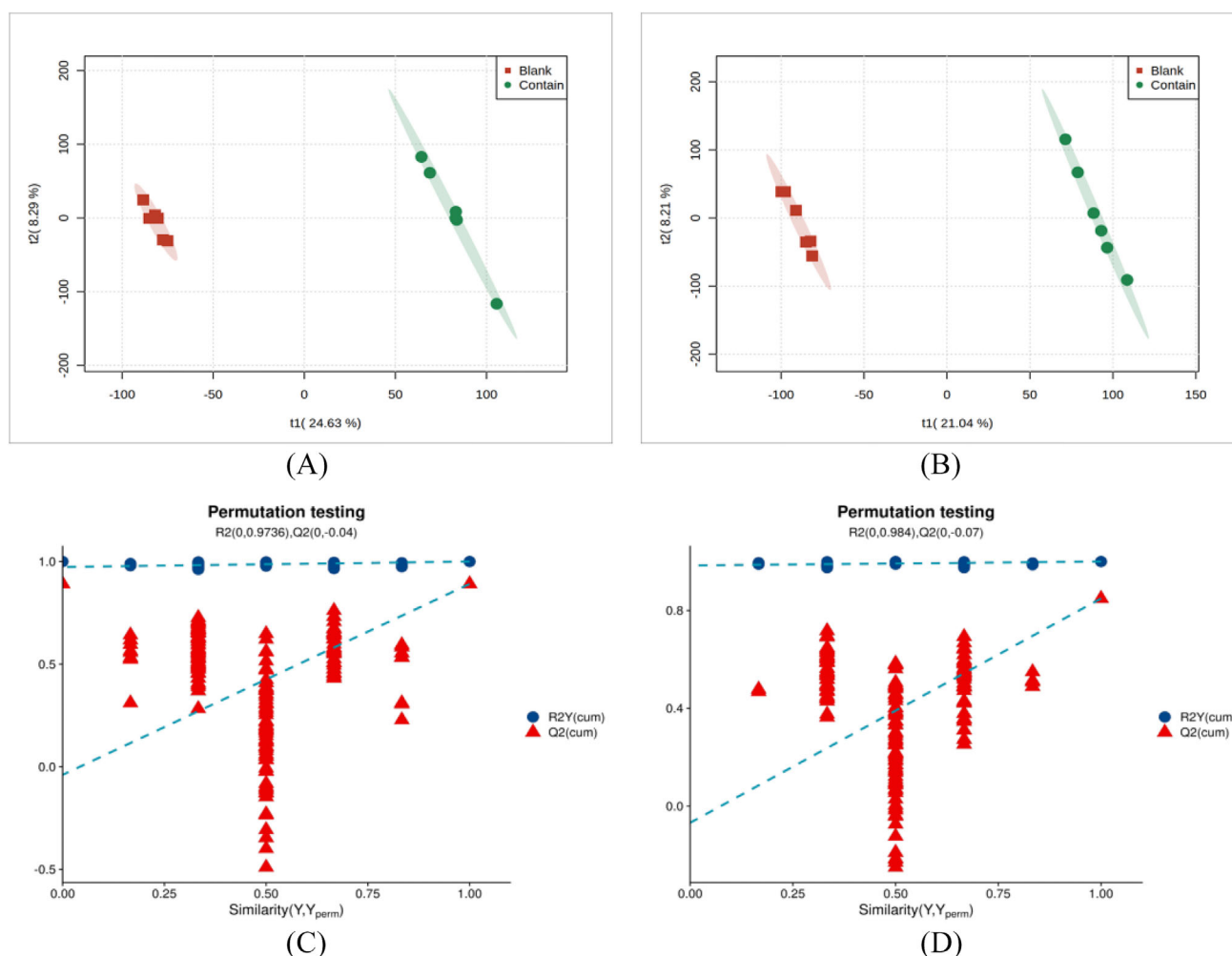


FIGURE 4 The results for PLS-DA models based on plasma. (A) The PLS-DA score plots in the positive ion mode. (B) The PLS-DA score plots in the negative ion mode. (C) The PLS-DA permutation tests in the positive ion mode. (D) The PLS-DA permutation tests in the negative ion mode.

2.4.4 | Hippocampus histopathology observation

The Hippocampus was isolated, fixed in 4% paraformaldehyde, embedded in paraffin and then cut into thin sections (about 5 μm).

The paraffin sections were stained with HE staining. The morphological changes of cells in the hippocampus tissues were observed and recorded using a colourized pathology image analyser.

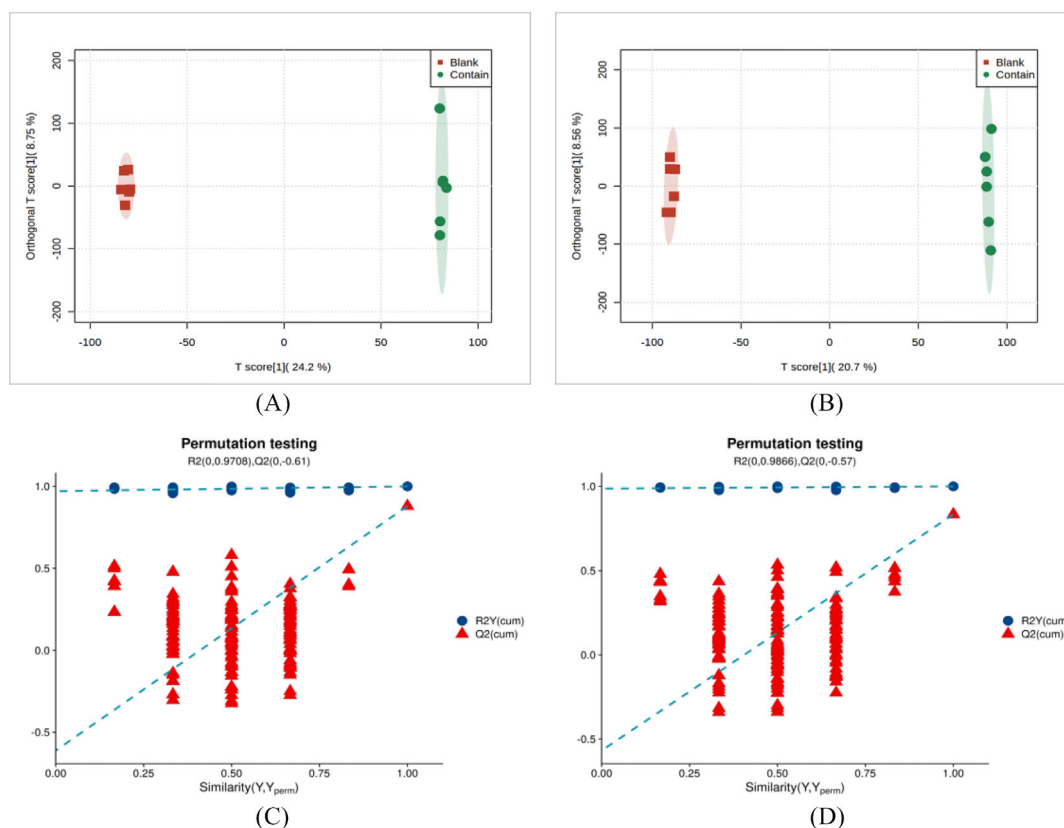


FIGURE 5 The results for OPLS-DA models based on plasma. (A) The OPLS-DA score plots in the positive ion mode. (B) The OPLS-DA score plots in the negative ion mode. (C) The OPLS-DA permutation tests in the positive ion mode. (D) The OPLS-DA permutation tests in the negative ion mode.

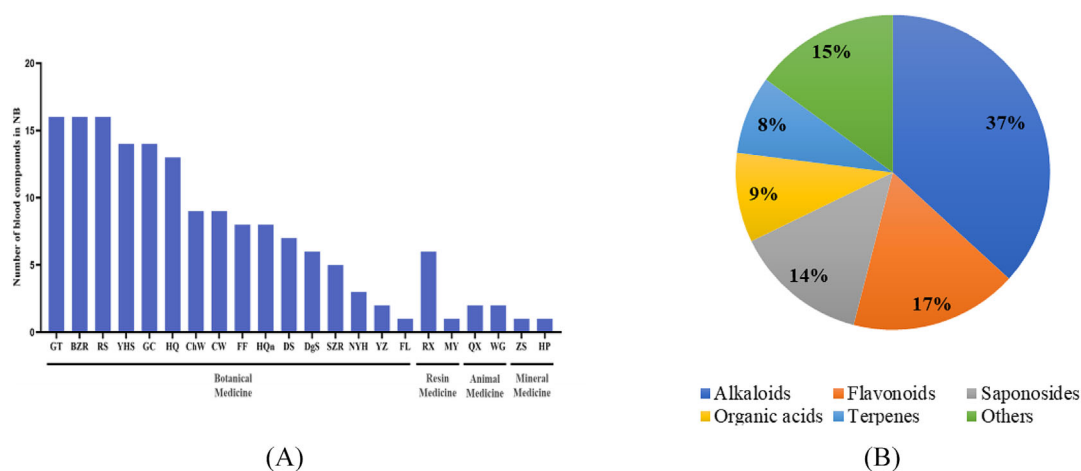


FIGURE 6 Chemical absorbed into blood identification of NBDC using UPLC-Q-TOF/MS. (A) The number of components for each herb. (B) Structural classification of compounds contained in NBDC. BZR, Boziren; ChW, Chuanwu; CW, Caowu; DgS, Dangshen; DS, Danshen; GC, Ganciao; FF, Fangfeng; FS, Fushen; GT, Gouteng; HQ, Huangqi; HQn, Huangqin; MY, Moyao; NYH, Naoyanghua; QX, Quanxie; RS, Renshen; RX, Ruxiang; SZR, Suanzaoren; WG, Wugong; YHS, Yanhusuo; YZ, Yuanzhi.

2.4.5 | Statistical analyses

SPSS 21.0 statistical software was used to analyse the data. Data on continuous variables conformed to a normal distribution with homogeneous variance and were expressed as the mean \pm standard deviation. The two-tailed Student's test for two groups analysis or one-way ANOVA for multiple groups analysis was used to compare differences between groups. $p < 0.05$, $p < 0.01$ and $p < 0.001$ were considered significant, statistically significant and highly significant, respectively.

2.5 | Relevance analysis

The Spearman correlation between serum metabolites and pharmacodynamic indicators was performed by the corr.test function from the pacman R package. We completed the correlation in those pharmacodynamic indicators and metabolites ($p < 0.05$, VIP > 1), which were found to be statistically significant between groups.

3 | RESULTS

3.1 | Analysis of NBDC chemical components in vivo and in vitro using UPLC-Q-Orbitrap-MS

3.1.1 | PCA

The TIC of the plasma samples in the blank, model and drug (high-dose) group in positive and negative ion mode are shown in Figure 2. The mass spectrometry detection data of NB capsules, blank plasma group, drug-containing plasma group and QC sample group were imported into SIMCA software and analysed by PCA, which showed that the QC samples clustered well together, indicating good instrument stability and reliable data results (Figure 3).

TABLE 3 Effect of NBDC on body weight of MA rats ($\bar{x} \pm SD$, $n = 10$).

Category	Initial weight	Final weight
Blank group	214.9 \pm 12.5	367.4 \pm 73.8
Model group	211.8 \pm 10.1	305.6 \pm 31.0 [#]
Low-dose group	211.5 \pm 22.3	329.4 \pm 53.9
Medium-dose group	213.6 \pm 10.9	350.8 \pm 59.9 [*]
High-dose group	214.0 \pm 11.4	356.3 \pm 42.5 ^{**}
Positive group	214.6 \pm 11.7	339.5 \pm 28.5 ^{**}

Note: VS blank group.

[#] $p < 0.05$, ^{##} $p < 0.01$; VS model group,

^{*} $p < 0.05$, ^{**} $p < 0.01$.

3.1.2 | PLS-DA

PLS-DA was applied to investigate the changes in plasma metabolites in the blank group and drug-containing group. The PLS-DA score plots were generated based on the metabolites detected in positive and negative ion modes (Figure 4A,B). The blank group and the drug-containing group were separated on both sides, proving significant differences in the chemical composition of the two groups of samples. The value of R²Y was 1.0, and Q² was 0.891 in positive ion mode. In negative ion mode, the value of R²Y was 1.0 and Q² was 0.849. The permutation tests for PLS-DA models are shown in Figure 4C,D. The above data prove that the model is stable and reliable with good prediction ability.

3.1.3 | Orthogonal projections to latent structures analysis (OPLS-DA)

OPLS-DA was applied to investigate the changes in plasma metabolites in the blank group and drug-containing group. The OPLS-DA score plots were generated based on the metabolites detected in positive and negative ion modes (Figure 5A,B). The blank and drug-containing groups were distinguished, implying that the between-group differences were more significant than the within-group differences and that the model could be used to screen for differential chemical compounds between the two groups. The value of R²Y was 1.0, and Q² was 0.851 in positive ion mode. In negative ion mode, the value of R²Y was 1.0, and Q² was 0.808. The permutation tests for OPLS-DA models are shown in Figure 5C,D. The above data prove that the model is stable and reliable with good prediction ability.

3.1.4 | Identification and analysis of absorbed components of NBDC

A total of 258 components in NB capsules were identified or tentatively characterized, 154 in positive ion mode and 104 in negative ion

TABLE 4 Effect of NBDC on the behaviour of MA rats ($\bar{x} \pm SD$, $n = 10$).

Category	CPP	Spontaneous activity	Stereotyped behaviour
Blank	428.25 \pm 107.46	102 \pm 27.3	0 \pm 0
Model	684.63 \pm 137.95 ^{##}	169 \pm 30.7 ^{##}	3.50 \pm 0.71 ^{##}
Low dose	590.50 \pm 88.36	138 \pm 26.3 [*]	2.60 \pm 0.70 ^{**}
Medium dose	544.38 \pm 96.40 [*]	132 \pm 28.1 ^{**}	2.50 \pm 0.85 ^{**}
High dose	483.63 \pm 100.05 ^{**}	124 \pm 32.5 ^{**}	2.40 \pm 0.84 ^{**}
Positive	517.00 \pm 129.43 [*]	120 \pm 35.5 ^{**}	2.00 \pm 0.82 ^{**}

Note: VS blank group,

[#] $p < 0.05$, ^{##} $p < 0.01$; VS model group,

^{*} $p < 0.05$, ^{**} $p < 0.01$.

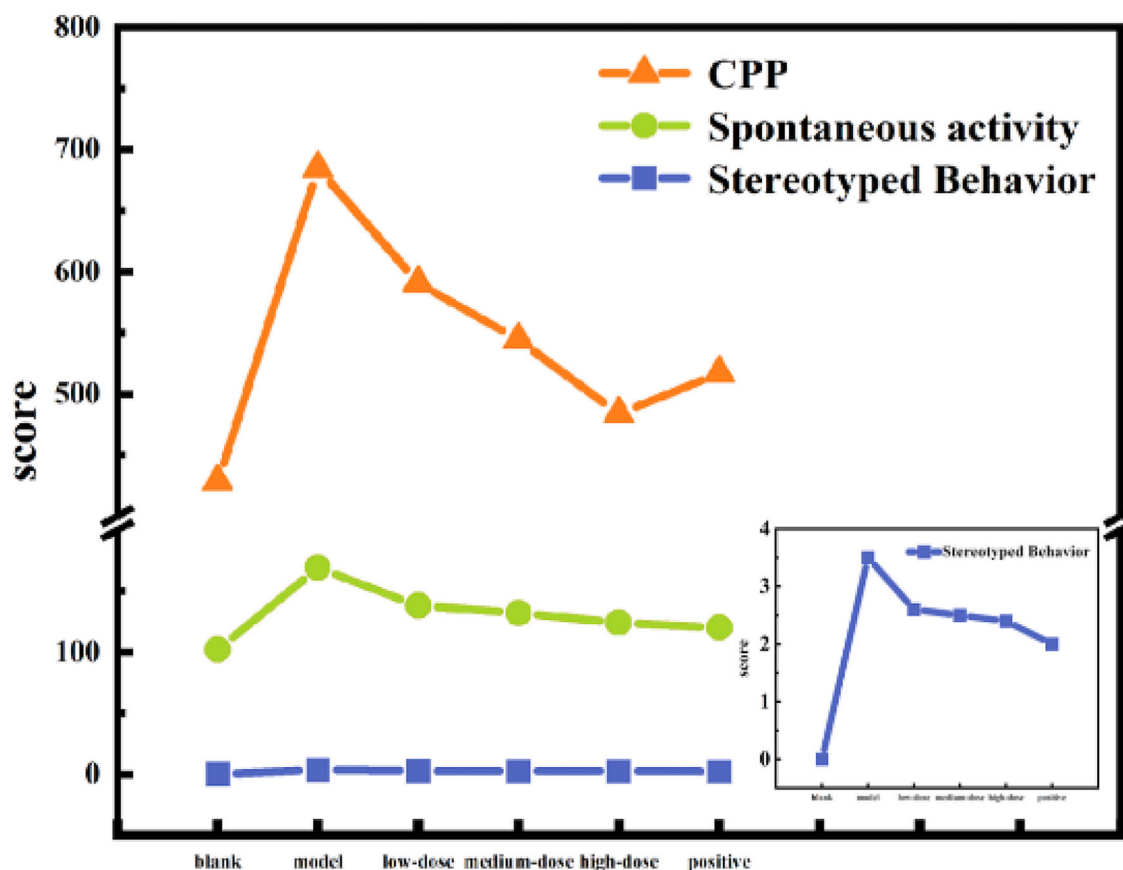


FIGURE 7 Effect of NBDC on the behaviour of MA rats.

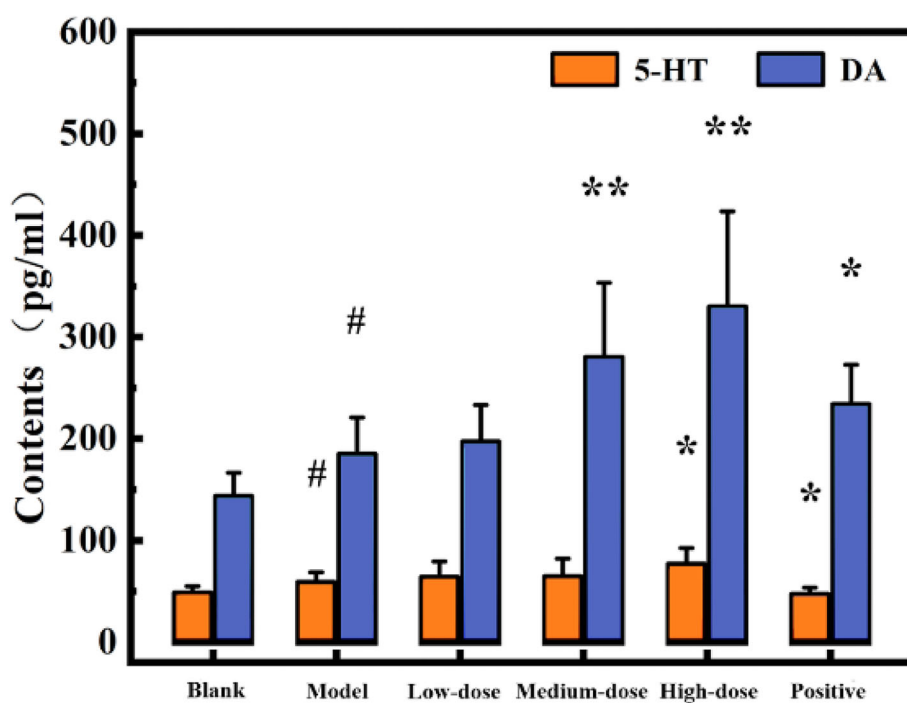


FIGURE 8 Effect of NBDC on the level of DA and 5-HT. VS blank group, # $p < 0.05$, ## $p < 0.01$; VS model group, * $p < 0.05$, ** $p < 0.01$.

mode. The difference compounds between the blank group and the drug-containing group were screened with criteria that the value of FC was more than 2, the VIP value was more than 1 and the p -value was less than 0.05. Compared with NBDC compounds, 87 components of prototype compounds in plasma were identified, 57 in positive and 30 in negative ion modes. The constituents absorbed into blood were mainly derived from the Zhichuanwu, Zhicaowu, Yanhusuo, Gouteng, Renshen and Gancao and mostly belonged to alkaloids, flavonoids and saponosides shown in Figure 6. The compound-specific information is shown in Table 2.

3.2 | Effect of NBDC on MA-addicted rats

3.2.1 | Effect on body weight

Compared to the blank group, the model group of rats demonstrated a significant reduction in body weight ($p < 0.05$). In contrast, both the medium and high dose groups, as well as the positive drug group, exhibited increased body weights relative to the model group ($p < 0.05$). These results suggest that NBDC can increase the body weight of MA-induced rats. The results are shown in Table 3.

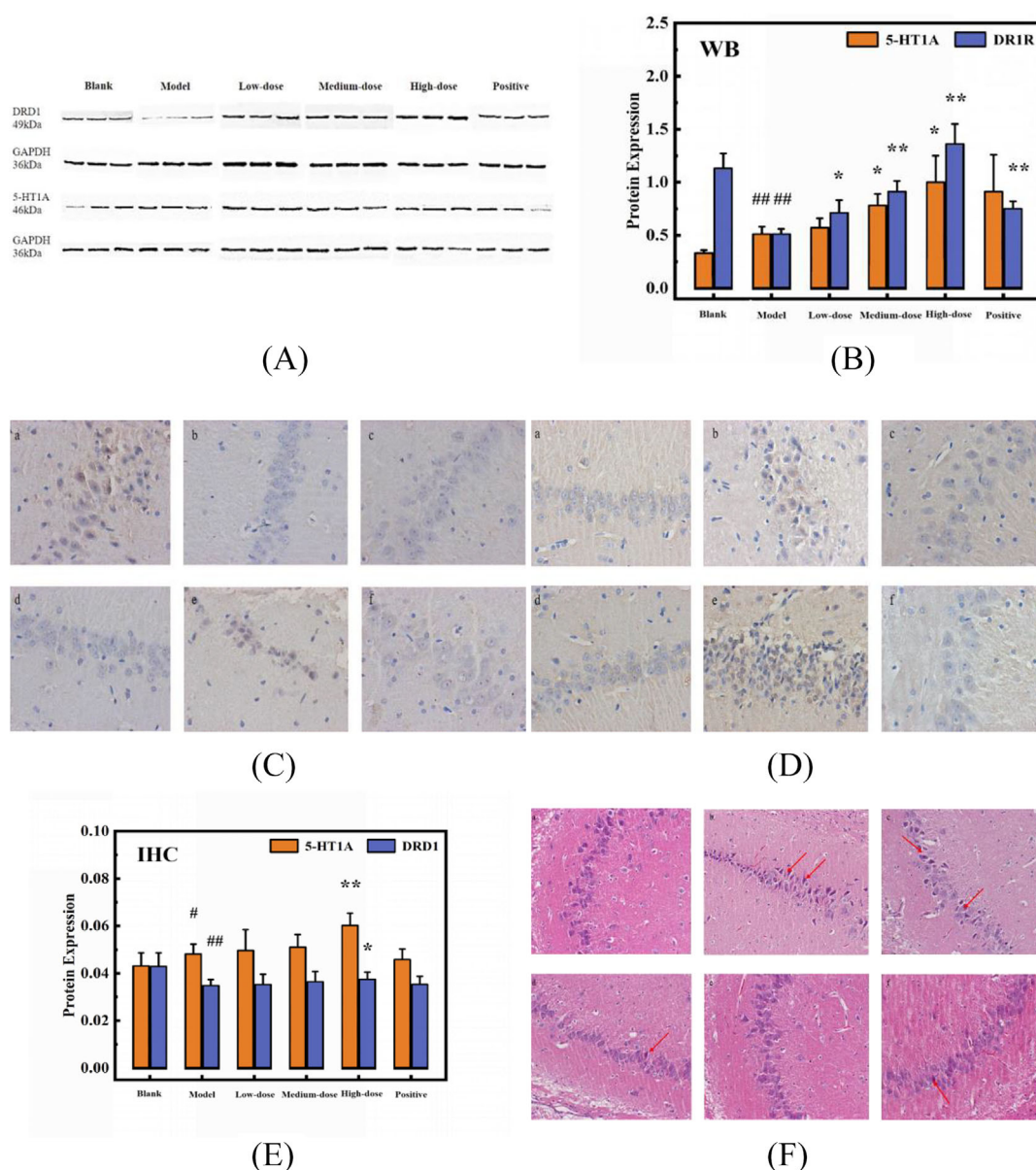


FIGURE 9 Effect of NBDC on the expression of DRD1 and 5-HT1A. The protein expressions were determined by WB and IHC analysis. Protein bands and IHC results were quantified by densitometry. (A) Protein bands. (B) Protein expression results measured by WB. (C) DRD1 positive expression results ($\times 400$). (D) 5-HT1A positive expression results ($\times 400$). (E) Protein expression results measured by IHC. (F) The HE staining hippocampus tissue micrographs ($\times 400$). (a) Blank group, (b) model group, (c) low-dose group, (d) medium-dose group, (e) high-dose group and (f) positive group. VS blank group, # $p < 0.05$, ## $p < 0.01$; VS model group, * $p < 0.05$, ** $p < 0.01$.

3.2.2 | Effect on ethology

The result of ethology is shown in Table 4 and Figure 7. An elevation in the CPP score was evident in the model group relative to the blank group ($p < 0.01$), indicating the development of a position-specific conditioned preference by the rats toward the drug-paired chamber. This confirms the successful establishment of the MA-induced rat model. Similarly, the number of spontaneous activities and the score of stereotyped behaviour increased in the model group compared with the blank group ($p < 0.01$). Subsequent treatment with NBDC or risperidone led to a significant reduction in three behavioural parameters, with trends toward normalization to levels observed in the blank group ($p < 0.05$). Conversely, the low-dose group showed no significant change in CPP scores compared to the model group ($p > 0.05$). Furthermore, the CPP score was found to be lower in the positive

control group compared to the high-dose group. Collectively, these outcomes suggest that high-dose NBDC effectively mitigates MA-induced CPP in rats, demonstrating a superior efficacy profile to risperidone.

3.2.3 | Effect on the concentration of DA and 5-HT in serum

DA and 5-HT are common biomarkers in addiction to MA.¹⁷ Figure 8 shows the alterations in serum concentrations of DA and 5-HT in rats before and after modelling and drug administration. Compared to the blank group, the model group exhibited a significant increase in both DA and 5-HT levels ($p < 0.05$). When compared with the model group, the DA levels were higher in the medium-dose, high-dose and positive

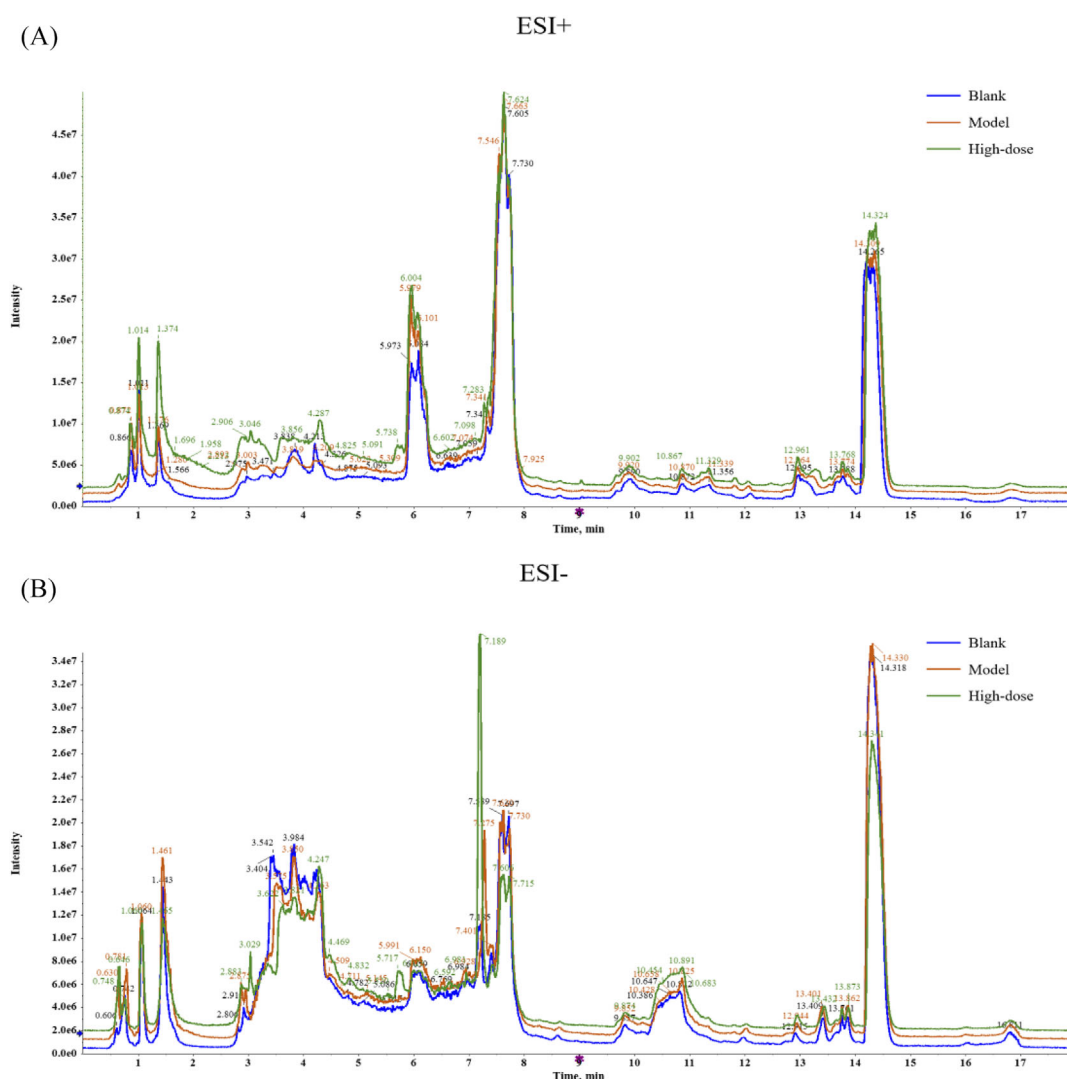


FIGURE 10 Total ion chromatograms in the positive and negative modes. (A) Positive model of plasma samples. (B) Negative model of plasma samples.

groups ($p < 0.05$), whereas the high-dose group showed an increase in 5-HT levels ($p < 0.05$), and the positive control group demonstrated a decrease in 5-HT levels ($p < 0.05$).

3.2.4 | Effect on the expression of DRD1 and 5-HT1AR in the hippocampus

To delineate the impact of NBDC on the dopaminergic and serotonergic systems within the hippocampus, western blot (WB) assays and

immunohistochemistry (IHC) staining techniques were employed to quantify the protein levels of dopamine receptor D1 (DRD1) and serotonin receptor 1A (5-HT1AR), respectively. The findings from both methodologies are concordant, as depicted in Figure 9A–E. MA exposure led to a significant downregulation of DRD1 levels relative to the blank group ($p < 0.01$). Post-treatment with NBDC or risperidone, there was a notable restoration of DRD1 protein expression compared to the model group ($p < 0.05$). Conversely, MA engendered an upregulation of 5-HT1AR protein expression compared with the blank group ($p < 0.05$), an effect which also appeared in the NBDC

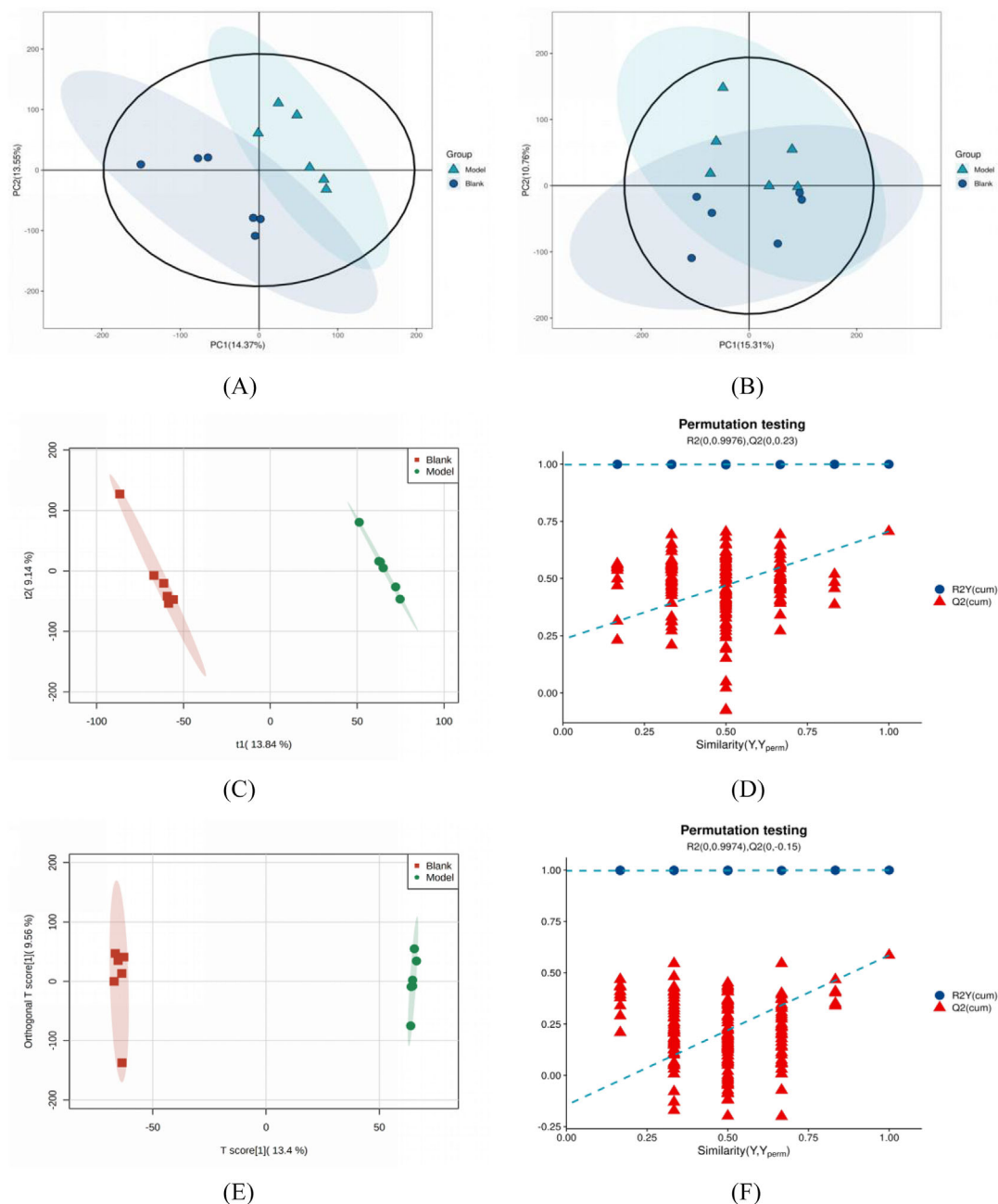


FIGURE 11 Multivariate statistical analysis of the metabolites in the rat plasma in the model group versus the blank group. (A) PCA score plot in the positive ion mode. (B) PCA score plot in the negative ion mode. (C) PLS-DA score plot in the positive ion mode. (D) PLS-DA permutation test in the positive ion mode. (E) OPLS-DA score plot in the positive ion mode. (F) OPLS-DA permutation test in the positive ion mode.

treatment group compared with the model group ($p < 0.05$). No discernible variation in 5-HT_{1A}R receptor expression was observed between the positive group and the model group ($p > 0.05$).

3.2.5 | Effect on cells morphological changes in the hippocampus

The morphological alterations induced by MA within hippocampal cells upon exposure were examined using phase-contrast microscopy to assess the therapeutic effects of NBDC. Microscopic observation revealed that rats administered with MA exhibited distinct histopathological disruptions, characterized by the disarray of pyramidal cells, intensified nuclear staining and a decline in the quantity of intact neurons, among other cellular anomalies. The hippocampal cell morphology in animals treated with NBDC progressively regained normalcy, as illustrated in Figure 9F. This suggests that NBDC possesses potential neurorestorative properties capable of mitigating the deleterious effects of MA on hippocampal architecture.

3.3 | Mechanism of NBDC relieving MA addiction based on metabolomics

3.3.1 | Total ion chromatogram of metabolomics of plasma

The TIC of the plasma samples in the blank, model and drug (high-dose) groups in positive and negative ion modes are shown in

Figure 10. After data preprocessing, comparing the RT and matching with HMDB databases, 614 and 525 compounds were identified from plasma samples in the positive and negative ion modes, respectively.

3.3.2 | Analysis of differential metabolites and metabolic pathways in MA addiction

Multivariate statistical analysis

The metabolites in the plasma samples of the model and blank groups were analysed by using PCA, and the model and blank groups were clearly distinguished in the positive ion model (Figure 11A), indicating that the chemical composition of the samples in the two groups was significantly different. However, there was no significant difference between the two groups in negative ion mode (Figure 11B). In the PLS-DA supervised model, the parameters of R²_Y and Q² were 1.0 and 0.706, respectively, in the positive ion mode and 1.0 and 0.436, respectively, in the negative ion mode. The parameters were R²_Y = 1.0, Q² = 0.586, and R²_Y = 1.0, Q² = 0.255, respectively, in positive and negative ion modes in the OPLS-DA supervised model. The above data indicates that the model is steady and trusty with excellent predictive ability in the positive ion model (Figure 11C-F). The data of this experiment were statistically analysed using the data under the positive ion model.

Differential metabolite screening

Differential metabolites were screened by the VIP value of the OPLS-DA model and the p -value of the t -test. Based on VIP > 1.0 and $p < 0.05$, 75 differential metabolites were screened between the

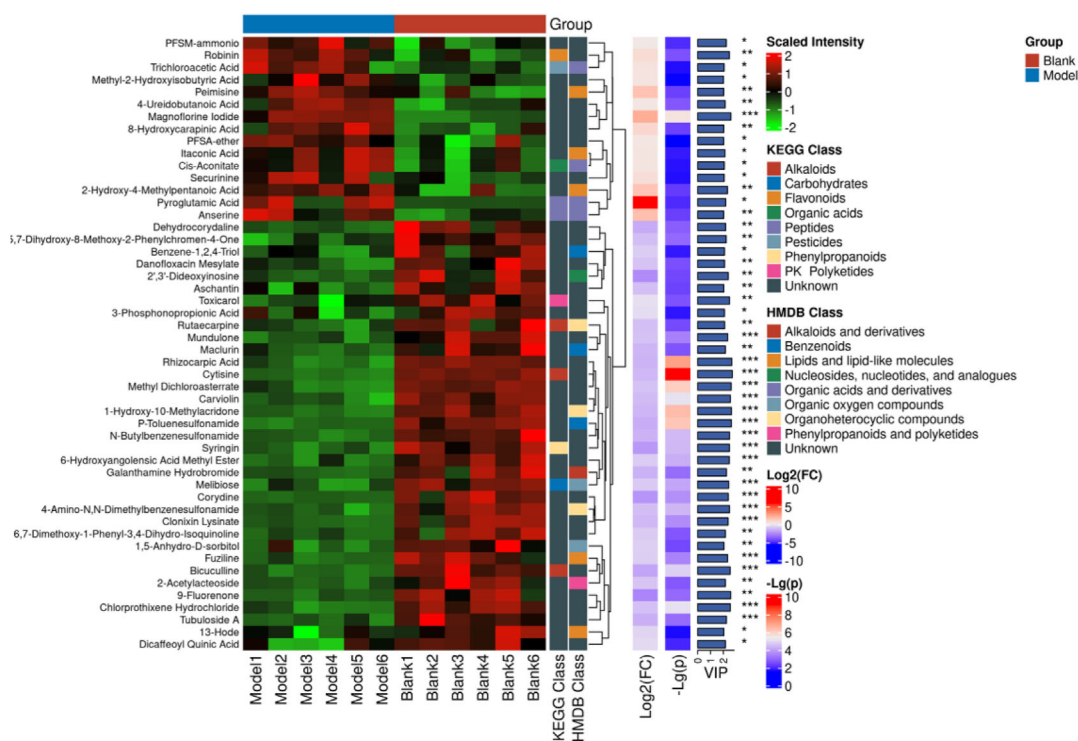


FIGURE 12 Heatmap of differential metabolites of the model group versus the blank group.

model and the blank groups in the positive ion mode. A total of 19 metabolites were upregulated ($FC > 1$), and 56 metabolites were downregulated ($FC < 1$). The top 50 differential metabolites with VIP values were selected for hierarchical cluster analysis, with up-regulation in red and down-regulation in green (Figure 12).

Potential biomarker prediction

The screened differential metabolites were subjected to functional analysis in HMDB and KEGG database. Finally, eight differential endogenous metabolites in the serum of MA-induced rats were confirmed as potential biomarkers of MA addiction and are shown in Table 5. Compared with the blank group, the levels of anserine, histidine, pregnenolone and 3-methylhistidine were increased. The levels of L-dopa, 1,5-anhydro-D-sorbitol, melibiose and norharman were decreased in the model group.

KEGG pathway analysis

To further explore the overall metabolic alterations during MA addiction, the data of screened differential metabolites were dealt with

the MetaboAnalyst platform for enrichment analysis and pathway analysis, matching with multiple metabolic pathways. The potential MA addiction pathways by the KEGG pathway analysis in the plasma are shown in Figure 13. The results showed that the main enrichment pathways for differential metabolites included cocaine addiction, amphetamine addiction and alcoholism. Among them, histidine and tyrosine metabolism had the smallest p -value, the highest significance and the most enriched metabolites.

3.3.3 | Analysis of differential metabolites and metabolic pathways in NBDC relieving effect on MA addiction

Multivariate statistical analysis

The metabolites in the model and drug groups' plasma samples were analysed by using PCA, PLS-DA and OPLS-DA. In the PCA unsupervised model, the model and drug groups were clearly distinguished in the positive ion model (Figure 14A) and the negative ion model

TABLE 5 Potential biomarkers of MA addiction.

MetaboName	KEGGID	HMDBID	RT (min)	m/z	Formula	FC	p-value	VIP	AUC
Anserine	C01262	HMDB0000194	14.122	241.1280	C ₁₀ H ₁₆ N ₄ O ₃	2.9642	0.005493	2.029086	0.944
Histidine	C00768	HMDB0000177	14.104	156.0763	C ₆ H ₉ N ₃ O ₂	2.1984	0.01052	1.904227	0.944
Pregnenolone	C01953	HMDB0000253	1.357	339.2352	C ₂₁ H ₃₂ O ₂	1.4812	0.037561	1.663903	0.833
3-Methylhistidine	C01152	HMDB0000479	14.067	170.0925	C ₇ H ₁₁ N ₃ O ₂	1.3974	0.044952	1.576194	0.833
L-dopa	C00355	HMDB0000181	12.109	198.0765	C ₉ H ₁₁ NO ₄	0.60518	0.017161	1.831069	0.889
1,5-Anhydro-D-sorbitol	C07326	HMDB0002712	10.444	165.0753	C ₆ H ₁₂ O ₅	0.55848	0.004051	2.055822	0.944
Melibiose	C05402	HMDB0000048	13.882	365.1090	C ₁₂ H ₂₂ O ₁₁	0.51737	9.78E-05	2.420271	1.000
Norharman	C20157	HMDB0012897	1.492	169.0746	C ₁₁ H ₈ N ₂	0.39183	0.03018	1.696126	0.917

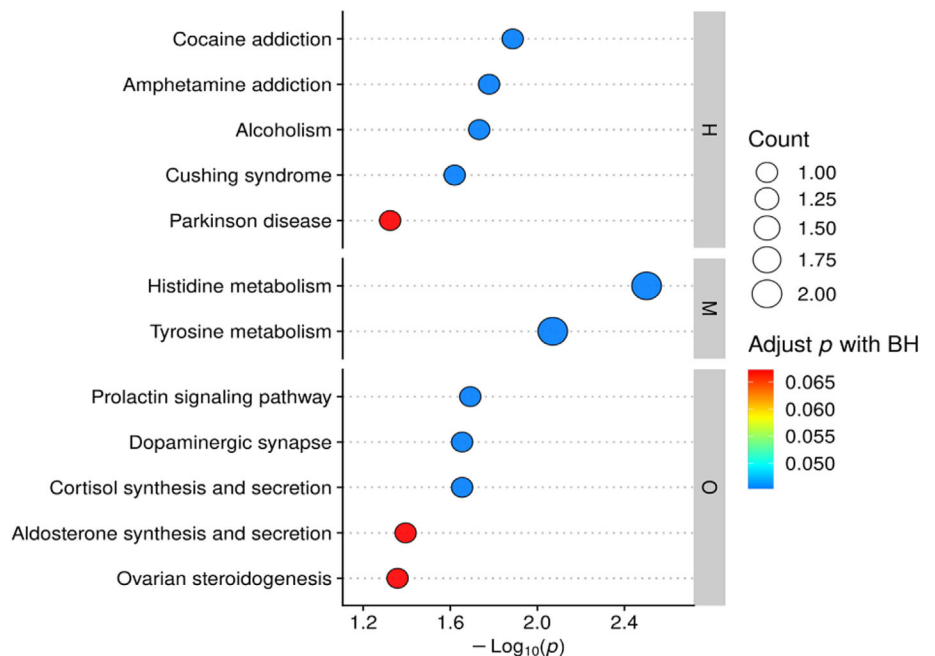


FIGURE 13 KEGG pathway enrichment bubble map of the model group versus the blank group.

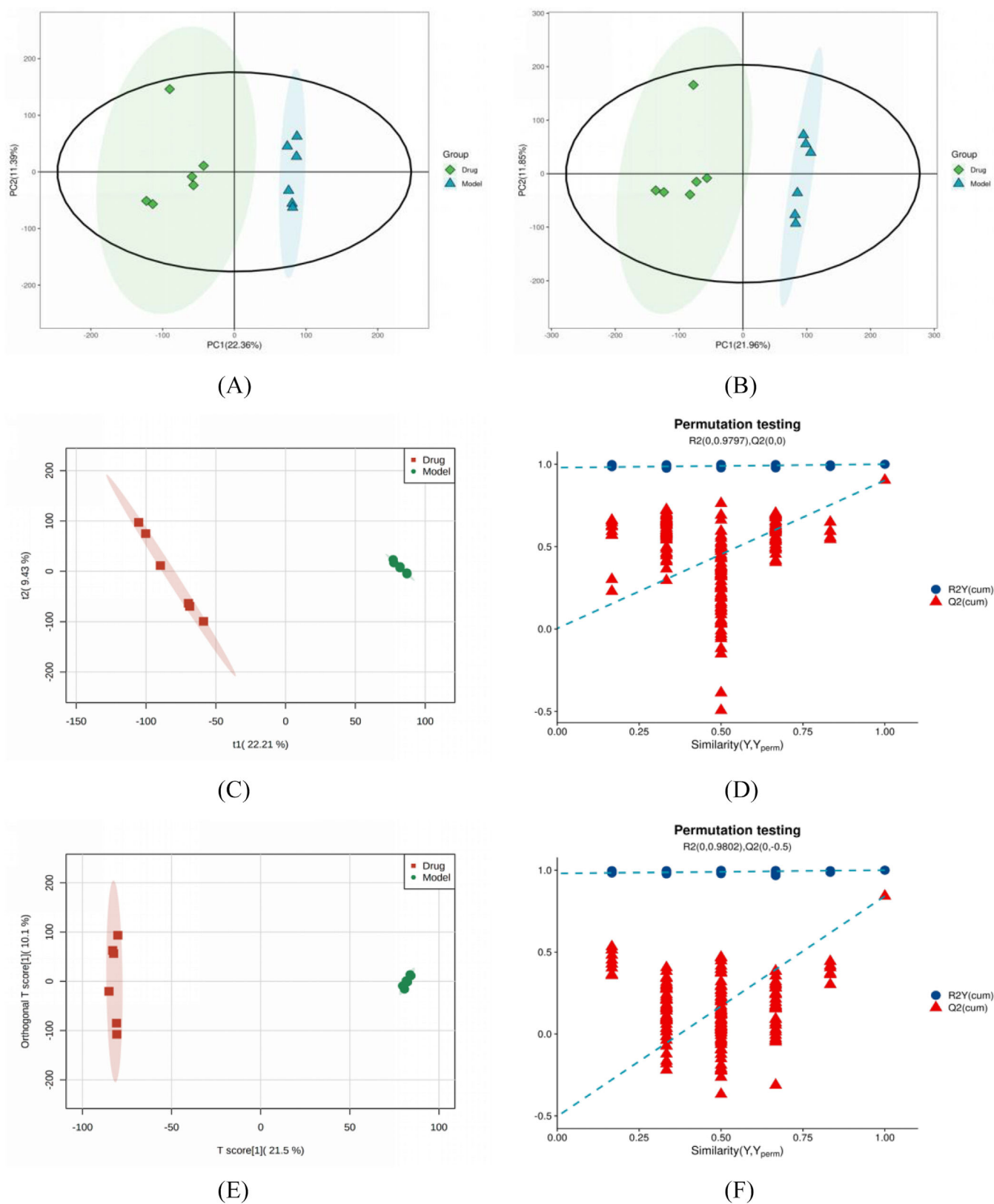


FIGURE 14 Multivariate statistical analysis of the metabolites in the rat plasma in the drug group versus the model group. (A) PCA score plot in the positive ion mode. (B) PCA score plot in the negative ion mode. (C) PLS-DA score plot in the positive ion mode. (D) PLS-DA permutation test in the positive ion mode. (E) OPLS-DA score plot in the positive ion mode. (F) OPLS-DA permutation test in the positive ion mode.

(Figure 14B), indicating that the composition of metabolites in the rat with MA addiction has been varied. The PLS-DA supervised model was steady and trusty, which can be confirmed by the parameters ($R^2Y = 1.0$, $Q^2 = 0.903$) based on the permutation test in the positive ion mode (Figure 14C,D). The OPLS-DA supervised model was also steady and trusty, which can be confirmed by the parameters ($R^2Y = 1.0$, $Q^2 = 0.916$) based on the permutation test in the positive ion mode (Figure 14E,F). The above data proved that the model is steady and trusty with excellent predictive ability in the positive ion model.

Differential metabolite screening

Differential metabolites were screened by the VIP value of the OPLS-DA model and the p -value of the t -test. Based on $VIP > 1.0$ and $p < 0.05$, 231 differential metabolites were screened in the positive ion mode between the drug and the model groups. A total of 156 metabolites were upregulated ($FC > 1$), and 75 metabolites were downregulated ($FC < 1$). The top 50 differential metabolites with the VIP value were selected for hierarchical cluster analysis, with up-regulation in red and down-regulation in green (Figure 15).

Potential biomarker prediction

The screened differential metabolites were subjected to functional analysis in HMDB and KEGG database. Finally, 26 differential endogenous metabolites in the serum of MA-induced rats were confirmed as potential biomarkers of MA addiction and shown in Table 6. Compared with the model group, the levels of 4-(beta-acetylaminoethyl) imidazole, norharman, cytidine 5'-diphosphocholine, 4-aminobenzoic acid, L-tyrosine, L-dopa, D-alanyl-D-alanine, dopamine, all-trans-

retinoic acid, L-theanine, 4-aminophenol, trimethylamine N-oxide, pregnenolone, 3-methylcrotonylglycine, 5'-methylthioadenosine, 4-guanidinobutyric acid, histidine, D-tryptophan and diethanolamine were increased, and the levels of palmitoylcarnitine, isoleucine, nicotinamide, homoarginine, lactose, bilirubin and tauroursodeoxycholic acid were decreased in the drug group.

KEGG pathway analysis

The potential NBDC relieving MA addiction pathways by the KEGG pathway analysis in the plasma are shown in Figure 16. The results showed that the main enrichment pathways for differential metabolites included cocaine addiction, amphetamine addiction, alcoholism, Parkinson's disease, tyrosine metabolism, prolactin signalling pathway and dopaminergic synapse. Among them, cocaine addiction and amphetamine addiction had the smallest p -value and the highest significance, and tyrosine metabolism had the most enriched metabolites.

3.4 | Relevance analysis

In order to gain a deeper understanding of the correlation between pharmacodynamic changes and metabolic changes, Pearson correlation analysis was conducted, revealing a significant association. The comprehensive correlation matrix presented in Figure 17 revealed a suite of robust correlations. The concentrations of DA and 5-HT exhibited positive relationships with D-alanyl-D-alanine, pregnenolone, histidine, 4-(beta-acetylaminoethyl) imidazole, cytidine 5'-diphosphocholine,

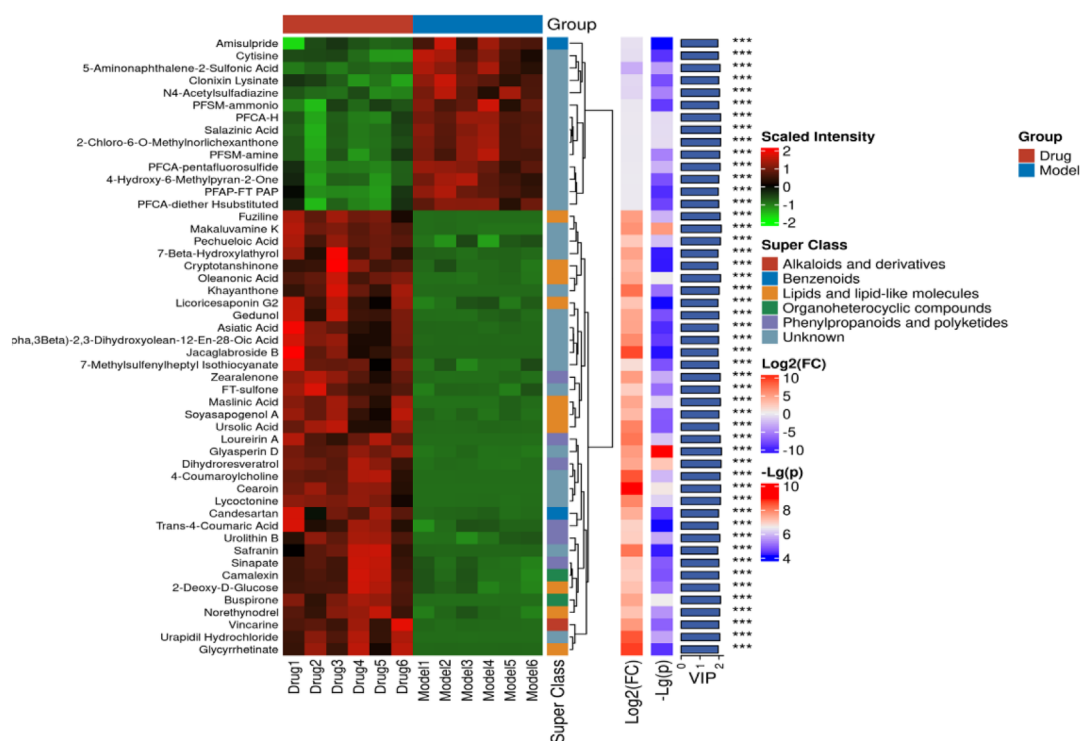


FIGURE 15 Heatmap of differential metabolites of drug group versus model group.

TABLE 6 Potential biomarkers of NBDC relieving MA addiction.

MetaboName	KEGGID	HMDBID	RT (min)	m/z	Formula	FC	p-value	VIP	AUC
4-(Beta-acetylaminoethyl)imidazole	C05135	HMDB0013253	9.091	154.0982	C ₇ H ₁₁ N ₃ O	31.138	0.001807	1.72043	1.000
Norharman	C20157	HMDB0012897	1.492	169.0746	C ₁₁ H ₈ N ₂	7.6287	0.04676	1.253166	0.861
Cytidine 5'-diphosphocholine	C00307	HMDB0001413	3.095	489.1137	C ₁₄ H ₂₆ N ₄ O ₁₁ P ₂	6.6772	0.013878	1.47139	0.972
4-Aminobenzoic acid	C00568	HMDB0304171	8.105	138.0543	C ₇ H ₇ NO ₂	6.4257	0.001056	1.78348	1.000
L-tyrosine	C00082	HMDB0000158	13.501	182.0804	C ₉ H ₁₁ NO ₃	5.0552	0.007055	1.567407	1.000
L-dopa	C00355	HMDB0000181	12.109	198.0765	C ₉ H ₁₁ NO ₄	4.573	0.004989	1.635747	1.000
D-alanyl-D-alanine	C00993	HMDB0003459	4.247	161.0897	C ₆ H ₁₂ N ₂ O ₃	3.9064	0.000203	1.879852	1.000
Dopamine	C03758	HMDB0000073	1.411	154.0856	C ₈ H ₁₁ NO ₂	3.6963	0.034915	1.309781	1.000
All-Trans-retinoic acid	C00777	HMDB0001852	1.043	301.2142	C ₂₀ H ₂₈ O ₂	3.6096	0.022441	1.418712	0.972
L-theanine	C01047	HMDB0034365	1.346	197.0898	C ₇ H ₁₄ N ₂ O ₃	2.9652	0.024138	1.382628	0.861
4-Aminophenol	C02372	HMDB0001169	1.92	110.0587	C ₆ H ₇ NO	2.2465	0.038997	1.277583	0.861
Trimethylamine N-oxide	C01104	HMDB0000925	12.151	76.07408	C ₃ H ₉ NO	2.2308	0.017984	1.442943	0.944
3-Methylcrotonylglycine	C20828	HMDB0000459	1.363	158.08	C ₇ H ₁₁ NO ₃	2.0337	0.043137	1.256371	0.889
5'-Methylthioadenosine	C00170	HMDB0001173	4.729	298.0977	C ₁₁ H ₁₅ N ₅ O ₃ S	2.0082	0.013067	1.491616	0.917
4-Guanidinobutyric acid	C01035	HMDB0003464	13.402	146.0914	C ₅ H ₁₁ N ₃ O ₂	1.997	0.020897	1.411608	0.889
Pregnenolone	C01953	HMDB0000253	1.357	339.2352	C ₂₁ H ₃₂ O ₂	1.7216	0.044212	1.259141	0.833
Histidine	C00768	HMDB0000177	14.104	156.0763	C ₆ H ₉ N ₃ O ₂	1.5702	0.011227	1.512861	1.000
D-tryptophan	C00525	HMDB0013609	1.376	265.0982	C ₁₁ H ₁₂ N ₂ O ₂	1.5693	0.014853	1.447167	0.944
Diethanolamine	C06772	HMDB0004437	11.205	106.0853	C ₄ H ₁₁ NO ₂	1.2566	0.047898	1.232078	0.861
Palmitoylcarnitine	C02990	HMDB0000222	6.976	400.3418	C ₂₃ H ₄₅ NO ₄	0.82807	0.048133	1.243401	0.833
Isoleucine	C16434	HMDB0033923	10.152	132.1006	C ₆ H ₁₃ NO ₂	0.81967	0.02163	1.407467	0.861
Nicotinamide	C00153	HMDB0001406	3.098	123.054	C ₆ H ₆ N ₂ O	0.65222	0.049083	1.261835	0.806
Homoarginine	C01924	HMDB0000670	13.944	189.1364	C ₇ H ₁₆ N ₄ O ₂	0.50328	0.022053	1.420501	0.861
Lactose	C00243	HMDB0041627	1.409	342.2998	C ₁₂ H ₂₂ O ₁₁	0.32251	0.001325	1.747266	1.000
Bilirubin	C00486	HMDB0000054	3.049	585.2700	C ₃₃ H ₃₆ N ₄ O ₆	0.27816	0.018751	1.43291	0.861
Tauroursodeoxycholic acid	C16868	HMDB0000874	4.563	522.2877	C ₂₆ H ₄₅ NO ₆ S	0.25756	0.016459	1.473301	0.944

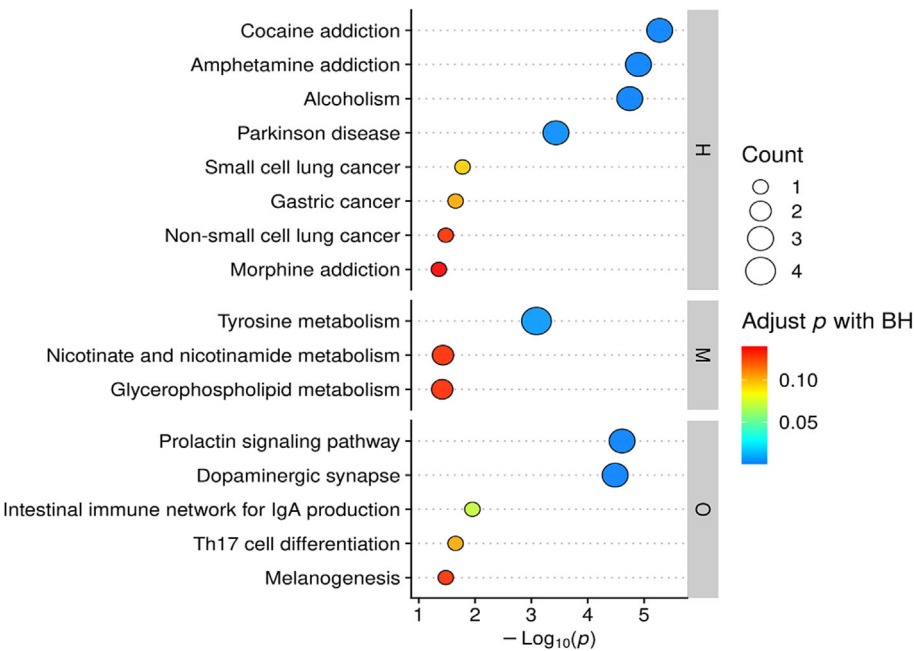


FIGURE 16 KEGG pathway enrichment bubble map of the drug group versus the model group.

4-aminobenzoic acid, dopamine and 5'-methylthioadenosine and inverse correlations with homoarginine, lactose and tauroursodeoxycholic acid, and so does 5-HT1AR. The ethology indicators of CPP and spontaneous activity were negatively correlated with trimethylamine N-oxide and 4-guanidinobutyric acid. These findings underscore the intricate network of biochemical interactions implicated in pharmacological responses and metabolic processes.

4 | DISCUSSION

The composition of Chinese medicine compounds is intricate, and the component absorbed into blood serves as the material basis for Chinese medicine to exert its medicinal effects and is also the key guarantee for the quality of Chinese medicine.^{18,19} In this investigation, 87 prototype compounds in NBDC were detected in the plasma. The present author's preliminary literature review has revealed that components such as l-tetrahydropalmatine, ginsenosides, rhyncho-phylline and astragaloside have shown promising effects in mitigating MA addiction.^{20,21} These components have also been identified in NBDC, and they can serve as Q biomarkers for the QC of NBDC compound formulations.

The CPP experiment, spontaneous locomotor activity experiment and stereotyped behaviour are currently the classical experimental models for evaluating psychiatric dependence on drugs.^{22,23} MA promotes the release of monoamine neurotransmitters, increases extracellular monoamine neurotransmitter concentrations and produces excitatory effects.²⁴ Therefore, monoamine neurotransmitters DA and 5-HT are both classical biomarkers of MA addiction, and DA receptors and 5-HT receptors are important targets for the treatment of MA addiction.¹⁷ This study found that NBDC could reduce the behaviour and psychiatric abnormalities induced by MA in rats in a dose-related

manner and NBDC also could increase DA and 5-HT levels and correlative receptor expression. MA promotes the release of monoamine neurotransmitters, including DA and 5-HT, from nerve terminals, thereby facilitating addiction via the reward system.²⁵ MA withdrawal causes significant emotional distress as DA and 5-HT are undergoing reductions. Increasing DA and 5-HT levels can ease withdrawal symptoms.²⁵ NBDC maintains the normal physiological state of the body by increasing DA and 5-HT levels to improve the withdrawal syndrome such as depression and cognitive impairment caused by the decrease of neurotransmitter levels after acute withdrawal and to reduce the drug-seeking cravings of users.

The metabolomics profiling elucidated showed that seven prominent KEGG signalling pathways were intricately associated with the mechanisms of MA addiction and NBDC therapeutic interventions. These pathways encompassed cocaine addiction, amphetamine addiction, alcohol addiction, Parkinson's disease, tyrosine metabolism, prolactin signalling and dopaminergic synapses. Specifically, within the amphetamine addiction metabolic pathway, three key endogenous metabolites—L-tyrosine, L-dopa and dopamine—were quantitatively identified. Moreover, an in-depth analysis of metabolite signatures revealed that five distinct endogenous substances were implicated in the histidine metabolic signalling pathway. This included histidine, anserine, histamine, 4-(β -acetylaminoethyl)imidazole (also recognized as N-acetylhistamine) and N-methyl-L-histidine (also known as 3-methylhistidine). Histamine H1 and H2 receptors stimulate dopamine D1 and D2 receptors, thereby facilitating the release of dopamine.²⁶ Conversely, the histamine H3 receptor exerts an inhibitory effect on dopamine synthesis.²⁷ It is speculated that NBDC may enhance the histamine level in vivo by enhancing the 'histidine \rightarrow histamine \rightarrow N-acetylhistamine' metabolic pathway, thereby promoting dopamine release and playing a role in intervening MA addiction. Neuroprotective effect of histamine H3 receptor

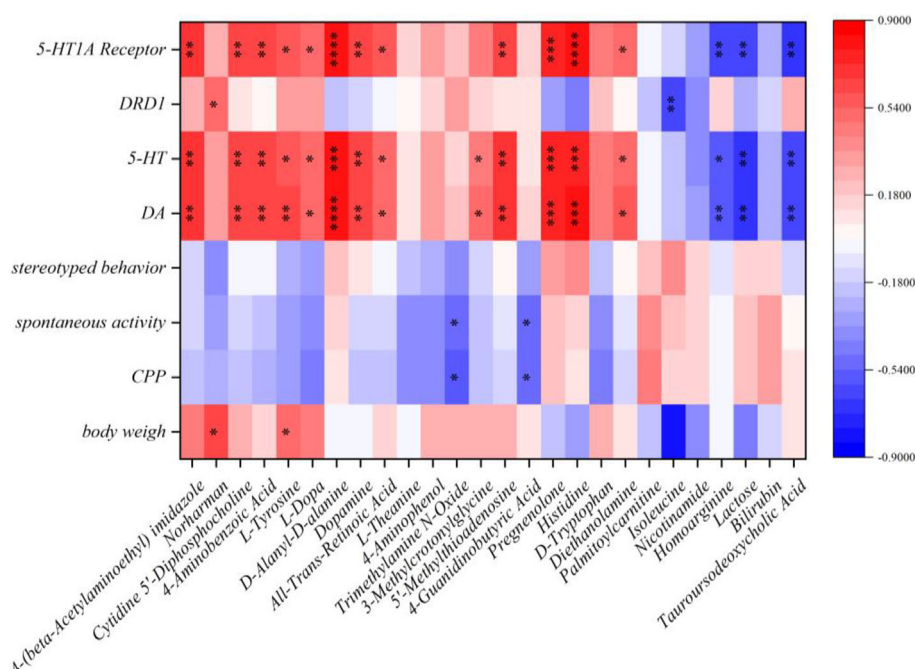


FIGURE 17 Correlation among metabolites and pharmacodynamic indicators. *, ** and *** represent $p < 0.05$, $p < 0.01$ and $p < 0.001$, respectively.

blockade on MA-induced cognitive impairment in mice.²⁸ Metoprine increasing the content of histamine attenuates MA-induced hyperlocomotion via activation of histaminergic neurotransmission in mice.²⁹ L-dopa, dopamine, histidine and histamine may serve as potential biomarkers of MA addiction, and histamine may serve as a potential action target for the treatment of MA addiction.

5 | CONCLUSION

In summary, NBDC ameliorates MA-induced behavioural abnormalities and alleviates MA withdrawal syndrome by acting on DRD1 and 5-HT1AR receptors and increasing neurotransmitter DA and 5-HT levels. Alkaloid components (e.g. benzoylmesaconine, uncarine, tetrahydroberberine, corydaline and L-tetrahydropalmatine) and saponin components (e.g. isoliquiritin, liquiritin, ginsenoside Rb3, ginsenoside Rb1 and licoricesaponin J2) were possibly the potential bioactive components of NBDC for relieving with MA addiction. Amphetamine addiction, tyrosine metabolism and dopaminergic synapse were possibly the critical metabolic pathways involved in alleviating MA addiction by NBDC. L-dopa, dopamine, histidine and histamine may serve as potential biomarkers of MA addiction, and histamine may serve as a potential target in the treatment of MA addiction.

ACKNOWLEDGEMENTS

The authors' sincere gratitude is delivered to Shanghai Bioprofile Technology Company Ltd., Shanghai, China, for their assistance in data analysis.

CONFLICT OF INTEREST STATEMENT

The authors declare that there are no conflicts of interest.

DATA AVAILABILITY STATEMENT

The authors confirm that the data supporting the findings of this study are available within the article and its supplementary materials.

STATEMENT ON THE INTEGRITY OF RESEARCH

This research was conducted in accordance with the Wiley Best Practice Guidelines on Research Integrity and Publishing Ethics.

ETHICS APPROVAL STATEMENT

The experimental protocol involving these animals was ethically reviewed and approved in accordance with internationally recognized guidelines for the care and use of laboratory animals, with the Ethics Approval Number 2021-0098.

CREDIT AUTHORSHIP STATEMENT

Bin Zhang is responsible for designing experimental protocols, executing experimental plans, processing data results and writing papers. Chen Yang and Zheng Yuxiao Zheng are responsible for executing the experiments. Xinliang Li is responsible for guiding the experiments. Xingguo Wang is responsible for providing the drug. Yuehui Li is responsible for formulating overarching research goals and aims.

ORCID

Bin Zhang  <https://orcid.org/0000-0002-4579-1075>

REFERENCES

1. Cruickshank CC, Dyer KR. A review of the clinical pharmacology of methamphetamine. *Addiction*. 2009;104(7):1085-1099. doi:[10.1111/j.1360-0443.2009.02564.x](https://doi.org/10.1111/j.1360-0443.2009.02564.x)
2. Shi Y, Wang F, Hu AZ, et al. Effects and mechanisms of Jinniu capsule on methamphetamine-induced conditioned place preference in rats. *Open Chem*. 2018;16(1):674-680. doi:[10.1515/chem-2018-0074](https://doi.org/10.1515/chem-2018-0074)
3. Dang DK, Shin EJ, Kim DJ, et al. Ginsenoside Re protects methamphetamine-induced dopaminergic neurotoxicity in mice via upregulation of dynorphin-mediated κ -opioid receptor and downregulation of substance P-mediated neurokinin 1 receptor. *J Neuroinflammation*. 2018;15(1):52. doi:[10.1186/s12974-018-1087-7](https://doi.org/10.1186/s12974-018-1087-7)
4. Fu KQ, Lin HY, Miyamoto Y, et al. Pseudoginsenoside-F-11 inhibits methamphetamine-induced behaviors by regulating dopaminergic and GABAergic neurons in the nucleus accumbens. *Psychopharmacology*. 2016;233(5):831-840. doi:[10.1007/s00213-015-4159-8](https://doi.org/10.1007/s00213-015-4159-8)
5. Liu L, Liu M, Zhao W, Zhao YL, Wang Y. Levo-tetrahydropalmatine: a new potential medication for methamphetamine addiction and neurotoxicity. *Exp Neurol*. 2021;344:113809. doi:[10.1016/j.expneurol.2021.113809](https://doi.org/10.1016/j.expneurol.2021.113809)
6. Zhou Y, Xiao S, Li C, et al. Extracellular vesicle-encapsulated miR-183-5p from rhynchophylline-treated H9c2 cells protect against methamphetamine-induced dependence in mouse brain by targeting NRG1. *Evid Based Complement Alternat Med*. 2021;2021:2136076. doi:[10.1155/2021/2136076](https://doi.org/10.1155/2021/2136076)
7. Zhang B, Li C, Guan Z, Li YH. 2022. Research Progress of Chinese Medicine in Treatment of Methamphetamine Dependence 24(10).
8. Liu R, Su C, Xu Y, et al. Identifying potential active components of walnut leaf that action diabetes mellitus through integration of UHPLC-Q-Orbitrap HRMS and network pharmacology analysis. *J Ethnopharmacol*. 2020;253:112659. doi:[10.1016/j.jep.2020.112659](https://doi.org/10.1016/j.jep.2020.112659)
9. Guan H, Li P, Wang Q, et al. Systematically exploring the chemical ingredients and absorbed constituents of *Polygonum capitatum* in hyperuricemia rat plasma using UHPLC-Q-Orbitrap HRMS. *Molecules*. 2022;27(11):3521. doi:[10.3390/molecules27113521](https://doi.org/10.3390/molecules27113521)
10. Gonzalez-Covarrubias V, Martinez-Martinez E, Del Bosque-Plata L. The potential of metabolomics in biomedical applications. *Meta*. 2022;12(2):194. doi:[10.3390/metabo12020194](https://doi.org/10.3390/metabo12020194)
11. Sheng W, Sun R, Zhang R, et al. Identification of biomarkers for methamphetamine exposure time prediction in mice using metabolomics and machine learning approaches. *Meta*. 2022;12(12):1250. doi:[10.3390/metabo12121250](https://doi.org/10.3390/metabo12121250)
12. Luo JH, Zou WS, Li J, et al. Untargeted serum and liver metabolomics analyses reveal the gastroprotective effect of polysaccharide from *Evodiae fructus* on ethanol-induced gastric ulcer in mice. *Int J Biol Macromol*. 2023b;232:123481. doi:[10.1016/j.ijbiomac.2023.123481](https://doi.org/10.1016/j.ijbiomac.2023.123481)
13. Yin TL, Pan YJ, Chen S, Zeng JN, Wang XG, Li YH. Clinical study of Nanbao Jieduqing capsule on methamphetamine abstinence syndrome with deficiency of Qi and Yin and accumulation of toxin and stasis. 2019;26(6):985-987.
14. Liu J, Hu Z, Liu D, Zheng A, Ma Q. Glutathione metabolism-mediated ferroptosis reduces water-holding capacity in beef during cold storage. *Food Chem*. 2023;398:133903. doi:[10.1016/j.foodchem.2022.133903](https://doi.org/10.1016/j.foodchem.2022.133903)
15. Li Z, Qi Y, Liu K, et al. Effect of Chaihu-jia-Longgu-Muli decoction on withdrawal symptoms in rats with methamphetamine-induced conditioned place preference. *Biosci Rep*. 2021;41(8):BSR20211376. doi:[10.1042/BSR20211376](https://doi.org/10.1042/BSR20211376)

16. Xu S, Tu S, Gao J, et al. Protective and restorative effects of the traditional Chinese medicine Jitai tablet against methamphetamine-induced dopaminergic neurotoxicity. *BMC Complement Altern Med*. 2018;18(1):76. doi:[10.1186/s12906-018-2094-z](https://doi.org/10.1186/s12906-018-2094-z)
17. Cao YY, Pu XP. Biomarkers of methamphetamine addiction and its measurements technique evolvement. *Chin J New Drugs*. 2019;28(1):34-39.
18. Yan Y, Li J, Zhang Y, et al. Screening the effective components of Suanzaoren decoction on the treatment of chronic restraint stress induced anxiety-like mice by integrated chinmedomics and network pharmacology. *Phytomedicine*. 2023;115:154853. doi:[10.1016/j.phymed.2023.154853](https://doi.org/10.1016/j.phymed.2023.154853)
19. Yang W, Zhang Y, Wu W, Huang L, Guo D, Liu C. Approaches to establish Q-markers for the quality standards of traditional Chinese medicines. *Acta Pharm Sin B*. 2017;7(4):439-446. doi:[10.1016/j.apsb.2017.04.012](https://doi.org/10.1016/j.apsb.2017.04.012)
20. Bin Z, Chao L, Zhimei G, Yuehui L. Research progress in the treatment of methamphetamine dependence with traditional Chinese medicine. *Modernization of Traditional Chin Med Mater Med-World Sci Technol*. 2022;24(10):3851-3861.
21. Zeng R, Pu HY, Zhang XY, Yao ML, Sun Q. Methamphetamine: mechanism of action and Chinese herbal medicine treatment for its addiction. *Chin J Integr Med*. 2023;29(7):665-672. doi:[10.1007/s11655-023-3635-y](https://doi.org/10.1007/s11655-023-3635-y)
22. Li X, Jiang F, Yao K, et al. Neuropeptide S attenuates methamphetamine-induced stereotyped behavior in rats. *Biochem Biophys Res Commun*. 2020;527(1):98-103. doi:[10.1016/j.bbrc.2020.04.085](https://doi.org/10.1016/j.bbrc.2020.04.085)
23. Tzschentke TM. Measuring reward with the conditioned place preference (CPP) paradigm: update of the last decade. *Addict Biol*. 2007;12(3-4):227-462. doi:[10.1111/j.1369-1600.2007.00070.x](https://doi.org/10.1111/j.1369-1600.2007.00070.x)
24. Shrestha P, Katila N, Lee S, Seo JH, Jeong JH, Yook S. Methamphetamine induced neurotoxic diseases, molecular mechanism, and current treatment strategies. *Biomed Pharmacother*. 2022;154:113591. doi:[10.1016/j.biopha.2022.113591](https://doi.org/10.1016/j.biopha.2022.113591)
25. Arias-Carrion O, Stamelou M, Murillo-Rodriguez E, Menendez-Gonzalez M, Poppel E. Dopaminergic reward system: a short integrative review. *Int Arch Med*. 2010;3(1):24. doi:[10.1186/1755-7682-3-24](https://doi.org/10.1186/1755-7682-3-24)
26. Zhuang QX, Xu HT, Lu XJ, et al. Histamine excites striatal dopamine D1 and D2 receptor-expressing neurons via postsynaptic H1 and H2 receptors. *Mol Neurobiol*. 2018;55(10):8059-8070. doi:[10.1007/s12035-018-0976-1](https://doi.org/10.1007/s12035-018-0976-1)
27. Aquino-Miranda G, Escamilla-Sanchez J, Gonzalez-Pantoja R, Bueno-Nava A, Arias-Montano JA. Histamine H3 receptor activation inhibits dopamine synthesis but not release or uptake in rat nucleus accumbens. *Neuropharmacology*. 2016;106:91-101. doi:[10.1016/j.neuropharm.2015.07.006](https://doi.org/10.1016/j.neuropharm.2015.07.006)
28. Luo H, Li X, Fan R, et al. Neuroprotective effect of histamine H3 receptor blockade on methamphetamine-induced cognitive impairment in mice. *Pharmacol Biochem Behav*. 2023a;222:173512. doi:[10.1016/j.pbb.2022.173512](https://doi.org/10.1016/j.pbb.2022.173512)
29. Kitanaka N, Hall FS, Kobori S, et al. Metoprime, a histamine N-methyltransferase inhibitor, attenuates methamphetamine-induced hyperlocomotion via activation of histaminergic neurotransmission in mice. *Pharmacol Biochem Behav*. 2021;209:173257. doi:[10.1016/j.pbb.2021.173257](https://doi.org/10.1016/j.pbb.2021.173257)

SUPPORTING INFORMATION

Additional supporting information can be found online in the Supporting Information section at the end of this article.

How to cite this article: Zhang B, Yang C, Zheng Y, Li X, Wang X, Yuehui L. Integration of pharmacochimistry, pharmacodynamics and metabolomics to reveal active ingredients and mechanism of Nan Bao detox capsule alleviating methamphetamine addiction. *Addiction Biology*. 2024;29(11):e70005. doi:[10.1111/adb.70005](https://doi.org/10.1111/adb.70005)